Published in final edited form as:

ACS Nano. 2019 November 26; 13(11): 12525–12539. doi:10.1021/acsnano.9b03050.

Nanoparticle-Based Hybrid Scaffolds for Deciphering the Role of Multimodal Cues in Cardiac Tissue Engineering

Junmin Lee[†,‡,§,⊥,+], **Vijayan Manoharan**[†,‡,∥,+], **Louis Cheung**[#], **Seungkyu Lee**[¶], **Byung-Hyun Cha**[†,‡,□], **Peter Newman**[†,‡], **Razieh Farzad**[†,‡], **Shreya Mehrotra**[†,‡,▽,★], **Kaizhen Zhang**[○], **Fazal Khan**[●], **Masoumeh Ghaderi**[†,‡], **Yi-Dong Lin**[⬡], **Saira Aftab**[†,‡], **Pooria Mostafalu**[†,‡], **Mario Miscuglio**[△], **Joan Li**[∥], **Biman B. Mandal**[▽], **Mohammad Asif Hussain**[■], **Kai-tak Wan**[○], **Xiaowu Shirley Tang**[*,#], **Ali Khademhosseini**[*,†,‡,§,⊥,▼,⬢], **Su Ryon Shin**[*,†,‡]

[†]Division of Engineering in Medicine, Brigham and Women's Hospital, Harvard Medical School, Cambridge, Massachusetts 02139, United States

[‡]Harvard-MIT Division of Health Sciences and Technology, Massachusetts Institute of Technology, Cambridge, Massachusetts 02139, United States

[§]Department of Bioengineering, Henry Samueli School of Engineering and Applied Sciences, University of California–Los Angeles, Los Angeles, California 90095, United States

[⊥]Center for Minimally Invasive Therapeutics (C-MIT), University of California–Los Angeles, Los Angeles, California 90095, United States

[∥]Australian Institute for Bioengineering and Nanotechnology, The University of Queensland, St Lucia, Brisbane, QLD 4072, Australia

[#]Department of Chemistry & Waterloo Institute for Nanotechnology, University of Waterloo, 200 University Avenue West, Waterloo, Ontario N2L 3G1, Canada

[¶]F. M. Kirby Neurobiology Center, Children's Hospital Boston, and Department of Neurobiology, Harvard Medical School, Boston, Massachusetts 02115, United States

[□]Division of Cardio-Thoracic Surgery, Department of Surgery, University of Arizona College of Medicine, Room 4302D, 1501 N. Campbell Avenue, Tucson, Arizona 85724, United States

[▽]Department of Biosciences and Bioengineering, Indian Institute of Technology Guwahati, Guwahati-781039, Assam, India

[*]**Corresponding Authors** tangxw@uwaterloo.ca (X. Tang)., khademh@ucla.edu (A. Khademhosseini)., shin4@bwh.harvard.edu (S. R. Shin).

[★]**Present Address** Centre for Nanotechnology, Indian Institute of Technology Guwahati, Guwahati-781039, Assam, India.

[+]Author Contributions

J.L. and V.M. contributed equally.

ASSOCIATED CONTENT

Supporting Information

The Supporting Information is available free of charge on the ACS Publications website at DOI: 10.1021/acsnano.9b03050. Additional figures including XPS, evaluation of the morphology with differential mechanical property, size effects of GO on cardiomyocyte morphology, comparison of organization on day 1, immunofluorescence images of cardiomyocytes stained for F-actin, vinculin, and nuclei on day 1 and 3, equation for upstroke velocity, APD50 and APD90, and qRT-PCR primer sequence information (PDF)

The authors declare no competing financial interest.

○Department of Mechanical and Industrial Engineering, Northeastern University, Boston, Massachusetts 02115, United States

●Department of Biochemistry, Faculty of Science, King Abdulaziz University, P.O. Box 80203, Jeddah 21589, Saudi Arabia

⬡Divisions of Genetics and Cardiovascular Medicine, Department of Medicine, Brigham and Women's Hospital, Harvard Medical School, Boston, Massachusetts 02115, United States

△Department of Electrical and Computer Engineering, George Washington University, Washington, D.C. 20052, United States

■Department of Electrical and Computer Engineering, King Abdulaziz University, Jeddah 21569, Saudi Arabia

▼Department of Chemical and Biomolecular Engineering, Henry Samueli School of Engineering and Applied Sciences, University of California–Los Angeles, Los Angeles, California 90095, United States

⬢Department of Radiology, David Geffen School of Medicine, University of California–Los Angeles, Los Angeles, California 90095, United States

Abstract

Myocardial microenvironment plays a decisive role in guiding the function and fate of cardiomyocytes, and engineering this extracellular niche holds great promise for cardiac tissue regeneration. Platforms utilizing hybrid hydrogels containing various types of conductive nanoparticles have been a critical tool for constructing engineered cardiac tissues with outstanding mechanical integrity and improved electrophysiological properties. However, there has been no attempt to directly compare the efficacy of these hybrid hydrogels and decipher the mechanisms behind how these platforms differentially regulate cardiomyocyte behavior. Here, we employed gelatin methacryloyl (GelMA) hydrogels containing three different types of carbon-based nanoparticles: carbon nanotubes (CNTs), graphene oxide (GO), and reduced GO (rGO), to investigate the influence of these hybrid scaffolds on the structural organization and functionality of cardiomyocytes. Using immunofluorescent staining for assessing cellular organization and proliferation, we showed that electrically conductive scaffolds (CNT- and rGO-GelMA compared to relatively nonconductive GO-GelMA) played a significant role in promoting desirable morphology of cardiomyocytes and elevated the expression of functional cardiac markers, while maintaining their viability. Electrophysiological analysis revealed that these engineered cardiac tissues showed distinct cardiomyocyte phenotypes and different levels of maturity based on the substrate (CNT-GelMA: ventricular-like, GO-GelMA: atrial-like, and rGO-GelMA: ventricular/atrial mixed phenotypes). Through analysis of gene-expression patterns, we uncovered that the engineered cardiac tissues matured on CNT-GelMA and native cardiac tissues showed comparable expression levels of maturation markers. Furthermore, we demonstrated that engineered cardiac tissues matured on CNT-GelMA have increased functionality through integrin-mediated mechanotransduction (*via* YAP/TAZ) in contrast to cardiomyocytes cultured on rGO-GelMA.

Graphical Abstract

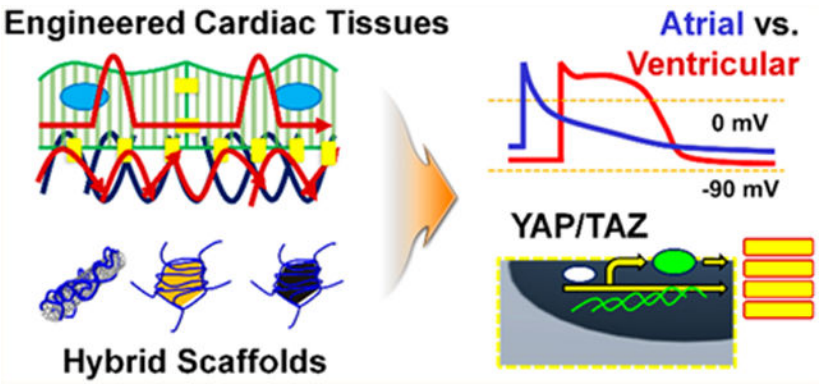

Keywords

carbon-based nanoparticles; cardiomyocytes; tissue engineering; extracellular matrix; gelatin methacryloyl; mechanotransduction

Cardiac muscle is composed of electrically and mechanically connected cardiomyocytes (~30% and ~60% in human and murine myocardium, respectively) intimately coupled to nonmyocytes such as fibroblasts, vascular smooth muscle cells, capillary endothelial cells, and macrophages.[1,2] Cardiomyocytes are the contractile cells of the heart, composing the atrial and ventricular chambers with expression of cardiac-specific markers such as cardiac troponin I and T, connexin 43 (Cx43), and sarcomeric α-actinin.[3] These cells play a crucial role in the propagation of electric signals throughout the specialized intracellular junctions and trigger the mechanical contractions that propel the blood.[4] Damaged cardiomyocytes are not replenished following events such as myocardial infarction due to their low proliferative capacity. As part of the compensatory mechanism, hypertrophic growth of remaining cardiomyocytes and cardiac fibrosis take place, which results in altered physiological function and pathological heart failure.[5,6] Current evidence suggests that engineered cardiac muscle tissue could restore the structural organization and functionality of the native tissue, thus holding great promise for improving the physiology of diseased hearts.[7,8] In this regard, well-informed design of scaffolds resembling the natural extracellular matrix (ECM) of myocardial tissue in terms of mechanical cues[9,10] and electrical stimulation[11] is crucial for the generation of cardiomyocytes with desired phenotype and enhanced functionality.

Hybrid scaffolds with homogeneously incorporated nanoparticles such as carbon nanotubes (CNTs),[12–16] graphene oxide (GO),[17–22] or gold (Au) nanowires[23,24] or nanoparticles[25–27] could address the major issues of commonly used porous scaffolds in myocardial tissue engineering.[28] First, they have good electrical conductivity comparable to the electrical conductivity of heart muscles, with a direct current (DC) estimated at 0.1 S/m. Second, they enable the formation of native ECM-like nanofibrous architecture capable of guiding cell fate decisions. Last, they possess better mechanical properties close to the native heart tissues (*e.g.*, mechanical property of primary human and adult murine cardiomyocytes is ~10 kPa[9] and ~10–40 kPa,[10] respectively). For example, previous works by our team showed that CNT-,[14,16] GO-,[19,29,30] or reduced GO (rGO)[17]-embedded gelatin methacryloyl (GelMA) hydrogels are capable of creating more *in vivo*-like microenvironments for cardiomyocytes,

thus enhancing the morphogenesis and contractility of neonatal cardiomyocytes. In a related study, Pok *et al.* fabricated CNT-incorporated chitosan-gelatin hydrogels as cardiac patches for cardiovascular defect repair, demonstrating enhanced contractility and functionality of cardiomyocytes mediated by CNTs in hydrogels that function as electrical nanobridges between cells.[13] Another study by Martins *et al.* showed that electrically conductive carbon nanofibers/chitosan composite scaffolds improved the properties of cardiac tissue constructs.[11] In addition, GO-based hydrogels were developed for regenerating bone,[22] controlling fibroblast cell behaviors,[31] or engineering cardiac tissues.[20,21] Despite these conscientious efforts, little understanding exists regarding how these nanoparticles with their distinct physical (mechanical, structural, and electrical) properties in the hybrid hydrogels can differentially regulate cardiac cell behaviors. For instance, GO and rGO are similar in shape while having major differences in surface chemistry and conductivity, and CNT and rGO have comparable conductivity but varied shapes and surface area. As a result, their interactions with cardiomyocytes are expected to induce different cell-regulatory mechanisms. Deciphering these mechanisms may also help elucidate myocardial regeneration.

Cardiac cells in their niche are known to have a built-in ability to sense and respond to physical surroundings through a process known as mechanotransduction.[32] Specifically, cardiomyocytes in the cardiac microenvironment interact with their ECM proteins through various integrins that can translate mechanical to biochemical information.[33] Mechanical forces—mediated by the integrin adhesions—and actin cytoskeleton—involved in the assembly and preservation of sarcomeres and myofibrils—could induce the activation of Yes-associated protein (YAP)/transcriptional coactivator with a PDZ-binding domain (TAZ) for cardiomyocytes to stimulate their proliferation and survival.[34,35] For instance, Xin *et al.* demonstrated that activation of YAP in the adult heart enhances cell proliferation and, therefore, promotes cardiac cell regeneration and their contractility after myocardial infarction.[36] However, it is known that the ability of YAP in driving cardiomyocyte proliferation decreases with their maturation.[37] Thus, we reasoned that comparing the ability of functional hybrid hydrogels incorporating different nanoparticles to induce increased cardiomyocyte functionality while sustaining their viability *in vitro* will provide insight into restoring function to the injured cardiac tissue. To this end, we incorporated CNTs, GO, and rGO into GelMA and created three hybrid scaffolds as cardiac cell culture platforms to explore how the physical properties of these nanoparticles differentially regulate cardiac cell behaviors.

RESULTS AND DISCUSSION

Fabrication and Physical Features of Hybrid Nanoparticles/Hydrogel Scaffolds.

Functional carbon-based nanoparticles (CBNs) with tunable mechanical, structural, and electrical properties are potential candidates in many areas related to biomedical applications, especially cardiac tissue engineering. To understand mechanisms underlying how the physical properties of different CBNs regulate cardiac cell behaviors on the hybrid scaffolds, we fabricated thin films of CNT-, GO-, and rGO-GelMA hybrid hydrogels (CBNs at a working concentration of 0.3% (w/v) in 7% (w/v) GelMA solution prepared by dilution

of a stock concentration of 0.5% (w/v) in 3.5% (w/v) GelMA solution with 12.25% (w/v) GelMA solution in 3:2 ratio) (Figure 1A). Homogeneous dispersion of CNTs and rGO was achieved through ultrasonic treatment in prepolymer solutions, followed by UV cross-linking.17,18 However, a thin film of GO-GelMA hydrogels was fabricated without the ultrasonic dispersion process, as GO sheets showed homogeneous dispersion in the GelMA prepolymer solution at ~80 °C.18 First, we confirmed the chemical compositions of CBNs using X-ray photoelectron spectroscopy (XPS), showing a good agreement with the previous reports (Figure S1).[17,38] The transmission electron microscope (TEM) image of CNTs and the atomic force microscopy (AFM) images of GO and rGO showed that (1) the CNT fiber diameter ranged from 15 to 45 nm (Figure 1B), (2) the sonicated rGO sheets were slightly smaller compared to the GO sheets but similar in shape, and (3) the size of both GO and rGO sheets was not uniform (Figure 1C,D). The thickness of the GO and rGO sheets was ~1.1 and ~8.4 nm, respectively, indicating that the reduction step-mediated interaction between individual sheets leads to stacking of several layers of rGO.[17] Scanning electron microscopy (SEM) images revealed the pore morphology of the hybrid scaffolds (Figure 1E–G). The smooth pore walls, regardless of CBN type, suggest that the CBNs were well-distributed inside the GelMA composite.[17] The pore size distribution of CBN-GelMA hybrid hydrogels revealed that CBNs lead to a microstructure with smaller pore sizes (CNT-GelMA: ~4.3 μm, GO-GelMA: ~5.3 μm, rGO-GelMA: ~5.1 μm) when compared to pristine GelMA gels (~15.7 μm) (Figure 1H). A histogram representing the pore size distribution of hybrid hydrogels was produced to look more closely at different effects of CBNs (quasi-1D CNTs *vs* 2D graphene sheets) on the hybrid gel porosity (Figure 1I). Unlike similar ranges of pore sizes mapped for GO- and rGO-GelMA, the pore size distribution of CNT-GelMA was shifted to the left (smaller sizes) with a narrower range, providing evidence for the nanoparticles' geometry-mediated regulation of pore sizes in hybrid hydrogels. Electrical conductivities of CBNs were also measured (Figure 1J). CNTs and rGO had relatively low electrical resistance due to the intrinsic conductivity of CNT (~100 kΩ/sq) and rGO (~1 kΩ/sq) networks, while pure GelMA and GO were electrically nonconductive (CBNs at a concentration of 0.3% (w/v)).

Topological, Mechanical, and Surface Properties of Hybrid Scaffolds.

To determine the surface roughness of pure and hybrid hydrogels, we carried out surface topographic mapping using AFM (Figure 2A). The surface of pure GelMA was smooth, while the CBN-GelMA hybrid hydrogel surfaces were rough, due to the presence of CBNs. Further, the surfaces of GO- and rGO-GelMA were relatively rougher than that of CNT-GelMA. This may be because, unlike well-dispersed one-dimensional (1D) CNTs in GelMA hydrogels, large-area 2D graphene sheets, especially multiple stacked rGO sheets after the reducing step, lead to the formation of uneven surface topography. In other words, varying 3D networks of CBNs in μm thick hydrogel films may affect different levels of roughness; the cross-linking of large-area 2D graphene sheets is likely to cause higher surface roughness compared to that of CNT-GelMA. To examine the role of CBNs in the local mechanical properties of hybrid hydrogels, we fixed the macroscale mechanical strength between the groups at around 6.5 kPa by controlling UV cross-linking time with fixed intensity (Figure 2F). Then, a Derjaguin–Muller–Toporov (DMT) modulus was obtained using the force–deformation plots to reveal the local mechanical properties of different

hybrid scaffolds (Figure 2B–E). Similar to the surface roughness of hybrid hydrogels, the samples containing rGO had the highest level of modulus fluctuation across the surface. Moreover, in line with previous studies showing the role of CBNs in reinforcements of hybrid hydrogels,[14,28] local elastic moduli of GelMA hydrogels incorporating CNTs (~16.8 kPa), GO (47.9 kPa), and rGO (~59.8 kPa) were higher than that of pure GelMA (~4.5 kPa) (Figure 2G). The higher values of Young's modulus for GO-GelMA and rGO-GelMA in comparison to CNT-GelMA could be attributed to the strength of stacked graphene nanosheets and the formation of uneven surface topography in hybrid scaffolds, which greatly affected the local modulus. Mechanical strength is one of well-known cues for the regulation of cellular behaviors such as morphology,[39] proliferation,[40] and differentiation.[41,42] In addition, it has been demonstrated that physiological stiffness of cardiomyocytes plays a crucial role in improving their functionality.[43] In this study, neonatal rat cardiomyocytes extracted from hearts (physiological stiffness ~10–40 kPa[10]) of 2-day-old pups were utilized. CNT-GelMA most resembled the mechanical cues of native neonatal rat cardiac tissue with a local mechanical property at ~16.8 kPa, exposing an inherent advantage[10] compared to other hybrid hydrogel substrates with similar bulk mechanical properties.

The protein adsorption at liquid/solid interfaces is a primary occurrence in several important processes including cell adhesion.[44] Moreover, hydrophobic surfaces are likely to adsorb more proteins, but less water compared to hydrophilic surfaces;[45] as a result, the balance between hydrophobicity/hydrophilicity in a scaffold would be important for cell culture. We assessed the protein adsorption (fetal bovine serum (FBS)) on the surface of hybrid hydrogels. Analysis of the FBS attachment onto hybrid hydrogels revealed that CNT-, GO-, and rGO-GelMA displayed ~1.2-fold, ~1.6-fold, and ~1.8-fold enhancements in the amount of absorbed proteins, respectively, compared to pure GelMA. These results indicate the CBNs embedded in GelMA hydrogels may lead to an increase in surface hydrophobicity. Moreover, increased surface roughness may play a role in the enhancement of absorbed protein amount,[46] but CNT-GelMA, which had smoother surfaces than those of GO- and rGO-GelMA, showed minimal effects (Figure 2H).

Cardiac Cell Organization and Proliferation on Hybrid Scaffolds.

To explore how CNT-, GO-, and rGO-GelMA differentially influence the organization of cardiomyocytes, we cultured freshly isolated neonatal cardiomyocytes on the hybrid scaffolds. Compared with cells on day 1, cardiomyocytes cultured for 5 days on different hybrid scaffolds showed CBN-dependent organization (Figure 3A). Cells cultured on CNT- and rGO-GelMA for 5 days displayed more cardiac muscle cell-like morphology with homogeneous, intact, well-elongated, and locally aligned morphology than those cultured on GO-GelMA. Morphological analysis revealed that cells cultured on hybrid hydrogels presented a variable spread area depending on CBN type (CNT-embedded: ~832.4 μm^2, GO-embedded: ~322.5 μm^2, rGO-embedded: ~780.3 μm^2) (Figure 3B). In addition, spreading of cells was also varied with the macroscale mechanical property of hybrid scaffolds (Figure S2) and size of CBNs (Figure S3). The cell spreading for cardiomyocytes on CNT-GelMA was larger than that on GO-GelMA likely due to (1) good electrical conductivity, (2) native heart tissue-like local mechanical properties, (3) smaller pore sizes, providing more binding

sites for cells, and (4) better uniformity, leading to lower surface roughness. Cardiomyocytes seeded on GO-GelMA displayed rounded morphology and globular structures in comparison to those cultured on CNT- and rGO-GelMA. To determine the morphological features of the cells, we assessed (1) the eccentricity, defined as deviation of a curve or orbit from circularity (1 is fully ellipse and 0 is round); (2) the form factor denoting how round a cell is (1 is fully round); and (3) the aspect ratio, denoting the ratio of major-axis to minor-axis length (Figures 4C–E and S4). For example, elongated cells have higher levels of eccentricity and aspect ratio, but a lower level of form factor compared to round cells. The eccentricity of cells on CNT-, GO-, and rGO-GelMA were ~0.97, ~0.74, and ~0.98, respectively (Figure 3C), in agreement with the result of the form factor, which were ~0.23, ~0.74, and ~0.34, respectively (Figure 3D). Cells on CNT-, GO-, and rGO-GelMA had aspect ratios of ~6.8, 1.6, and 5.3, respectively (Figure 3E). GO- and rGO-GelMA substrates with CBNs of similar shapes albeit different chemistry promoted significantly varied cell morphologies, indicating that the geometric shapes of CBNs in GelMA hydrogels played a minor role in dictating cellular shape compared to their chemical composition and hence their electrical conductivity, thus having an active role in cytoskeletal rearrangement through assembly and preservation of sarcomeres and myofibrils. We also seeded primary cardiac fibroblasts along with cardiomyocytes on the hybrid hydrogels to evaluate the biocompatibility of the scaffolds. Mitochondrial metabolic activity of cardiac fibroblasts was checked by the MTS assay, showing that the hybrid hydrogels, irrespective of CBN type, could promote a metabolically active state of fibroblasts for 5 days in culture (Figure 3F). However, DNA content analysis of the metabolically active cardiomyocytes cultured for 5 days revealed that CNT-GelMA scaffolds helped maintain higher viability of cardiomyocytes during their maturation compared to GO- (~1.7-fold, ~2.1-fold, and ~2.0-fold on day 1, 3, and 5, respectively) and rGO-GelMA (~1.5-fold, ~1.2-fold, and ~ 1.2-fold on day 1, 3, and 5, respectively) (Figure 3G). However, we acknowledge that cardiac fibroblasts (CFs) contamination during the isolation of cardiomyocytes (CMs) could have contributed towards the DNA content. Nevertheless, these findings suggest that CNT-GelMA, with distinct physical features from GO- and rGO-GelMA, may provide a more viable microenvironment for cardiomyocytes during maturation *in vitro,* and cell retention mediated by different hybrid scaffolds (*e.g.,* higher levels of CF and CM retention on CNT-GelMA compared to those on GO- and rGO-GelMA) might also influence their phenotypes and maturation. Since it is obvious that multimodal cues on the hybrid scaffolds could modulate both cell retention and cardiac tissue maturation, which are two interdependent factors, our hypothesis that different hybrid scaffolds could regulate the maturation of cardiac tissues by modulating their structural organization and functionality is still proven to be viable.

Regulation of Cardiomyocyte Phenotypes on Hybrid Scaffolds.

In this work, we hypothesized that the physical properties of CBNs could differentially influence cardiac cell properties on hybrid scaffolds. In order to test the above hypothesis, first, we examined whether the organization and proliferation of cardiac cells on various hybrid scaffolds are different. Further, the phenotypes of cardiomyocytes on hybrid scaffolds were evaluated by immunostaining of focal adhesion marker (vinculin) on day 3 and representative cardiac markers (sarcomeric α-actin, Cx43, and troponin I) on day 5 (Figures

4A–C and S5). Proteins associated with mechanosensing include integrin, vinculin, and α-actinin.[47] Expression of Cx43 indicates electrical and metabolic coupling between cells, and levels of troponin I links to the maturation of the contractile apparatus in cardiac cells (Figure 4D). It is expected that different hybrid scaffolds would differentially regulate cardiomyocyte phenotypes. The immunofluorescence staining results showed that the engineered cardiac tissues matured on CNT- and rGO-GelMA had notably higher expression levels of these markers compared to cells cultured on GO-GelMA: for the intensity of vinculin, cells on CNT-GelMA (~1.5-fold) and rGO-GelMA (~1.6-fold) showed higher expression (Figure 4E), for the length of sarcomeric α-actin, cells on CNT-GelMA (~1.8-fold) and rGO-GelMA (~1.4-fold) displayed longer lengths of sarcomeres (Figures 4F and S6), for the intensity of Cx43, cells on CNT-GelMA (~2.3-fold) and rGO-GelMA (~3.0-fold) exhibited higher expression (Figure 4G). However, for the intensity of troponin I, cardiomyocytes cultured on CNT-GelMA represent 1.3-fold and 1.5-fold higher expression relative to those cultured on GO- and rGO-GelMA, respectively (Figure 4H). These results indicate that the electrically conductive hybrid scaffolds functioning as electrical nanobridges between cardiomyocytes could promote higher expression levels of cardiac markers. However, the increase in troponin I expression is only observed in cells cultured on CNT-GelMA, suggesting that CNT-mediated reduction of pore sizes and better local mechanical properties in conjunction with electrical conductivity could further tailor the construction and maturation of functional, engineered cardiac tissues.

Electrophysiological Features of Engineered Cardiac Tissues on Hybrid Scaffolds.

Since we demonstrated that the cardiomyocytes on CNT-GelMA expressed higher levels of cardiac markers while maintaining their viability (~2.04-fold and ~1.21-fold higher amount of DNA on day 5 compared to GO- and rGO-GelMA, respectively, in Figure 3G), we then questioned whether these findings are associated with electrophysiological properties. To answer this, we first performed patch clamp recording to measure spontaneous action potential, which plays a role in initiating, regulating, and coordinating cardiac tissue contraction.[48] There are mainly three types of cardiomyocytes in the heart, which are nodal/pacemaker, atrial, and ventricular myocytes; separating these populations is valuable for cardiac evaluation, cell therapies, and drug development purposes.[49] The atrial and ventricular myocytes display putative steps (Figure 5A),[48] which are a rapid depolarization (phase 0), a partial repolarization (phase 1), a plateau stage (phase 2), another repolarization (phase 3), and a true resting membrane potential (phase 4). Comparative variations in conductance (through rapid Na^+/slow Ca^{2+} and K^+) and currents primarily determine the action potential in atrial and ventricular myocytes.[50] Ventricular action potential showed a longer duration and higher plateau potential in phase 2 due to “the balance between Ca^{2+} influx via voltage-gated slow Ca^{2+} channels and K^+ efflux through delayed rectifier K^+ channels (Figure 5A).[51] We measured action potentials across different conditions, and the results showed that cardiomyocytes matured on CNT-GelMA exhibited notably rapid upstroke velocity (~3.8 V/s) and a longer action potential period evaluated at 50% (APD50: action potential duration at 50% of the amplitude, ~0.62 s) and 90% (APD90: action potential duration at 90% of the amplitude, ~0.81 s), while the cells on GO- and rGO-GelMA displayed slow upstroke velocity (~0.62-fold for GO-GelMA and ~0.39-fold for rGO-GelMA) and shorter duration (APD50: ~0.58 s and ~0.45 s and APD90: ~0.77 s and

~0.73 s for GO- and rGO-GelMA, respectively) (Figures 5B–G and S6). Based on the duration and action potential plateau in phase 2, the cardiomyocytes cultured on CNT-GelMA and GO-GelMA most closely mimic ventricular myocytes and atrial myocytes, respectively; interestingly, cardiomyocytes cultured on rGO-GelMA displayed intermediate characteristics between the ventricular and atrial phenotypes. These findings suggest that different properties of CBNs in the hybrid scaffolds may play an important role in guiding cardiomyocyte fate decision. CNTs showed higher electrical conductivity, native ECM-like nanofibrous architecture with smaller pore sizes, and closer mechanical properties to native heart tissues, which enables cardiomyocytes to have better morphology and express higher levels of cardiac markers, resulting in the cells being more like ventricular myocyte phenotypes *in vitro.* Generating ventricular phenotypes is highly desirable because the scar tissue after myocardial infarction leads to ventricular dysfunction through electrical uncoupling of cardiomyocytes in the infarct regions.[52] However, cardiomyocytes on GO-GelMA hydrogels, which are electrically nonconductive (at a GO concentration of 0.3% (w/v)) and locally stiffer, may become articular-like myocytes.

To further examine the electrophysiological functions of cardiomyocytes cultured on different hybrid hydrogels, excitation thresholds and spontaneous beating frequency of the engineered cardiac tissues were assessed. Excitation thresholds of cardiomyocytes cultured on CNT- and rGO-GelMA were lower (~0.5- to 0.6-fold differences in the range of applied frequency, 0.5–3 Hz) compared to those cultured on GO-GelMA (Figure 5H). Since gas generation and local pH gradient—induced by high electric potential on the electrode surface in an aqueous electrolyte—are known to result in damage to engineered cardiac tissues,[16] a lower excitation potential is beneficial to regulate the contractile property of cardiac tissues for avoiding such damage. Recordings of spontaneous beating were utilized to track the progression of cardiac maturation and to analyze how different substrates preserved the contractility (Figure 5I). Unlike engineered cardiac tissues on CNT- and rGO-GelMA, which were capable of being paced by electric stimulation after day 1, those cultured on GO-GelMA could only be paced after 2 days in culture. In addition, the contraction frequency of cardiomyocytes on GO-GelMA decayed from 2.0 (on day 2) to 0.3 Hz (on day 3). However, prolonged increase in the beating frequency of cardiomyocytes was observed on cells cultured on CNT- and rGO-GelMA substrates for up to 5 and 8 days, respectively. This ability of CNT-GelMA substrates to sustain the spontaneous beating for more than a week could be attributed to their local mechanical property closely mimicking the native tissue microenvironment.

Inhibition of Contractility on Different Hybrid Scaffolds.

We demonstrated that cardiomyocytes cultured on electrically conductive CBN-laden scaffolds show enhanced contractility and spontaneous beating compared to those cultured on nonconductive GO-GelMA. To elucidate the signaling mechanisms underlying cardiomyocyte contractility, we employed blebbistatin, known as a myosin II inhibitor, which reduces the contractile motion of cardiomyocytes.[53] When cardiomyocytes were exposed to blebbistatin, the cells became smaller and displayed dendritic morphology; however, when the drug was removed, the cells could spread back and were able to make intercellular connections (Figure 6A). To evaluate the effect of blebbistatin on cell

morphology, we compared the area covered by cells with and without the treatment of blebbistatin. For this, cardiomyocytes were seeded and allowed to attach on the hybrid scaffolds for 24 h. Then the drug was administered for 24 h (24–48 h) and removed for the next 24 h (48–72 h), and this cycle was repeated once more (exposure: 72–96 h and removal: 96–120 h). We then measured the covered area every 24 h. As a control, we cultured cardiomyocytes on hybrid scaffolds in the absence of blebbistatin, showing that the covered area of cells increased with increasing culture time due to continuous cell growth (Figure 6B). In line with the result seen in Figure 3B, the areas of cells seeded with the same density were higher when cultured on CNT- and rGO-GelMA than that on GO-GelMA. In the presence of blebbistatin, the cell area slightly decreased, but it recovered and increased again when the drug was removed (Figure 6C). We found that inhibition of the contractile apparatus leads to a decrease in cardiomyocyte spread area regardless of CBN type, implying that activation of actomyosin contractility may not play a differential role in cardiac tissue contraction on different hybrid scaffolds. It is well known that mechanotransduction pathways starts from the integrin-mediated cell–ECM interaction and subsequently establish a positive feedback loop between integrin engagement and actomyosin contractility.[33] Consequently, we suspected that the type of nanoparticle incorporated in hybrid scaffolds affected the integrin engagement of cardiomyocytes differentially, thus guiding cardiac maturation with distinct downstream signaling.

Phenotypic Comparison with Native Cardiac Tissue *in Vivo* and Expression of Integrin Receptors.

Before proceeding by the addressing the question related to the integrin-mediated cell–ECM interaction, we compared cardiomyocytes cultured on CNT- and rGO-GelMA with native cardiac tissue. The reason we decided to mainly focus on the comparison between cardiomyocytes on CNT- and rGO-GelMA was that the electrically conductive scaffolds were shown to guide the cells to have better morphology and increased functionality. Quantifications of Cx43, sarcomeric α-actin, and troponin I expression were performed using real-time quantitative reverse transcription–polymerase chain reaction (qRT-PCR). After 5 days of incubation, the phenotypes of engineered cardiac tissues matured on CNT- and rGO-GelMA were evaluated and compared with native cardiac tissues; (1) for Cx43, cardiomyocytes cultured on CNT- and rGO-GelMA showed a ~62.7-fold and ~55.7-fold enhanced expression, respectively, (2) for sarcomeric α-actin, cardiomyocytes cultured on CNT- or rGO-GelMA expressed 5.41-fold higher or 0.05-fold lower levels, respectively, but (3) for troponin I, 0.03-fold and 0.05-fold decreased expression levels were displayed for cardiomyocytes cultured on CNT- and rGO-GelMA, respectively. These results revealed that engineered cardiac tissues matured on CNT-GelMA showed improved expression of cardiac markers except for troponin I compared with native cardiac tissues. For the expression level of troponin I, different signaling pathways may be associated with the cardiomyocytes matured on CNT-GelMA (integrin-mediated mechanotransduction, as shown in Figure 8) and native cardiac tissues (e.g., other signaling *in vivo* ranging from growth factor signaling to cell–cell adhesion), leading to differences in functionality and maturation. Moreover, based on the different expression levels of cardiac markers, the cells cultured on CNT-GelMA seem to be governed by different signaling mechanisms from those cultured on rGO-GelMA.

To address the question regarding the integrin engagement of cardiomyocytes on hybrid hydrogels containing different CBNs, we studied their expression of integrin receptors responsible for mechanotransduction initiating intracellular signaling. Cardiomyocytes were cultured for 3 and 5 days on CNT- and rGO-GelMA followed by qRT-PCR analysis of various integrin subunits (α1, α2, α3, α5, α7, and β1) (Figure 7D). Interestingly, cardiomyocytes cultured on CNT-GelMA display higher expressions of α1 (~2.5-fold), α2 (~3.3-fold), α3 (~1.1-fold), and β1 (~l.3-fold) on day 3 and α1 (~2.3-fold), α2(~l.5-fold), α3 (~l.6-fold), and β1 (~l.3-fold) on day 5 than those cultured on rGO-GelMA, which exhibit higher expression for α5 (~2.2-fold and ~l.3-fold on day 3 and 5, respectively) and α7 (~5.9-fold and ~l.2-fold on day 3 and 5, respectively) integrin. Cells interact with their ECM proteins through various integrins, and combinations of integrin α and β subunits specify the surface receptors that recognize ECM proteins such as laminin, fibronectin, vitronectin, and collagen.[54] In this study, we employed GelMA hydrogels derived from denaturing type 1 collagen.[55] Cells primarily bind to GelMA/collagen through the common integrin heterodimers, $\alpha1\beta1$ or $\alpha2\beta1$.[54] A previous study showed that $\alpha1\beta1$ could promote cell proliferation.[56] In addition, it was demonstrated that expression of integrin β1 receptor increases during the maturation process of cardiomyocytes in cardiac tissue engineering.[57] Cardiomyocytes cultured on CNT-GelMA—compared to those cultured on rGO-GelMA—show higher expression levels of distinct integrin receptors (*e.g.,* $\alpha1\beta1$ and $\alpha2\beta1$). This distinct integrin engagement possibly leads to differential signaling pathways and transcriptional regulation involved in mechanotransduction, which may influence their survival and maturation.

CNT-GelMA Guiding Cardiomyocyte Maturation through Enhanced Integrin Expression.

Cardiomyocytes cultured on CNT- and rGO-GelMA showed distinct levels of integrin and cardiac marker expression during maturation. To gain insight into how integrin adhesions affected downstream actin cytoskeletal rearrangement on different hybrid scaffolds and subsequently influenced the maturation of cardiomyocytes, we analyzed gene expression profiles pertinent to mechanotransduction, cytoplasmic structure, and growth (Figure 8A). A panel of transcripts linked to cytoplasmic structure and Rho family displayed higher levels of expression in cells cultured on CNT-GelMA on day 3; however no significant difference was detected on day 5. Cells cultured on CNT-GelMA for 3 days showed similar expression levels of mechanotransduction-related transcripts (focal adhesion and YAP/TAZ) to those cultured on rGO-GelMA However, intriguingly on day 5, engineered cardiac tissues matured on CNT-GelMA exhibited a much higher expression level of those transcripts (Vinculin, YAP/TAZ). It was reported that small GTPase Rho indirectly regulates YAP/TAZ activation by inducing the assembly of actin stress fibers in regard to the spreading of cells across the ECM.[58] This indicates that cardiomyocytes cultured on CNT-GelMA may (1) provide more point of contact for cell binding, thus upregulating integrin receptors (mainly $\alpha1\beta1$ and $\alpha2\beta1$), (2) spread on the scaffolds with proper mechanical cues (within physiological stiffness) and electrical conductivity, (3) form actin bundles and actomyosin stress fibers to activate Rho family, (4) establish positive feedback loops to activate YAP/TAZ in late stages of cardiomyocyte maturation, and (5) enhance cell proliferation by the activation of YAP. This mechanotransduction process for cardiomyocytes cultured on CNT-GelMA could induce better maturation while preserving their high functionality.

With the observed differences in the cardiac marker expression profiles between cardiomyocytes cultured on CNT- and rGO-GelMA, we sought to demonstrate if engineered cardiac tissues on CNT-GelMA would likewise possess enhanced gene expression associated with mechanotransduction signaling pathways, even when compared to native cardiac tissues. Expression of the transcripts employed above were again compared between engineered cardiac tissues matured on CNT-GelMA for 5 days and native cardiac tissues (Figure 8B). Similar to the trend shown in Figure 8A, engineered cardiac tissues matured on CNT-GelMA expressed higher degrees of genes associated with mechanotransduction and growth. We observed notably higher levels of YAP/TAZ (~4.6-fold for YAP and ~1.9-fold for TAZ) and SRC (~1.6-fold) as well as RhoA (~1.9-fold)/Rac1 (~4.5-fold) for cardiomyocytes matured on CNT-GelMA. It has been shown that the activation of SRC,[59] RhoA,[60] and Rac1[61] increases YAP transcriptional activity and the gene expression associated with YAP. These results may also demonstrate that mechanotransduction through YAP/TAZ played pivotal roles in enhanced functionality of engineered cardiac tissues on CNT-GelMA. We also saw a notably higher expression level of melusin (~2.6-fold) for engineered cardiac tissues on CNT-GelMA compared to *in vivo* cardiac tissues. Brancaccio *et al.* revealed that melusin, known as a muscle-specific protein, interacts with the cytoplasmic domain of β1 integrin and a mechanosensor transducing signal.[62] A related study by Unsöld *et al.* showed that high expression of melusin is associated with reduced fibrosis and apoptosis as well as enhanced cardiomyocyte contractility; specifically, cardiac rupture could be protected, and functional remodeling of cardiomyocytes with preserved myocyte contractility could be improved.[63] Taken together, these results reveal that engineered cardiac tissues matured on CNT-GelMA could have enhanced functionality through integrin-mediated mechanotrasduction *(via* YAP/TAZ), which is different from that of cardiomyocytes cultured on rGO-GelMA.

Furthermore, the present study provides insight into the design of a better hybrid scaffold for further *in vivo* applications that can more efficiently promote the maturation and proper phenotype of cardiomyocytes. Of the physical parameters studied, electrical conductivity had the most pronounced effect on the behavior of myocytes. In addition, matrix properties such as mechanical property, pore size, and roughness also played a subtle yet significant role in deciding the functionality of the cardiomyocytes. As shown in Figure 8C, conductive CNT-GelMA scaffolds with (1) mechanical property mimicking the native heart tissues, (2) smaller pore size providing more cell-binding sites, and (3) better uniformity leading to lower roughness could guide cells into ventricular phenotypes with increased functionality through integrin-mediated mechanotransduction *(via* YAP/TAZ).

CONCLUSION

Using GelMA hydrogels containing different carbon-based nanoparticles (CNTs, GO, and rGO), as we previously reported,[17,18] we fabricated hybrid cardiac tissues, while modulating the physical properties such as mechanical, structural, and electrical features in a facile way. Using these platforms, we show how CNT-, GO-, and rGO-GelMA differentially regulate the structural organization and functionality of cultured cardiomyocytes. In particular, we demonstrated that CNT networks have good electrical conductivity and native ECM-like nanofibrous architecture with better local mechanical properties resembling the native heart

tissue,[10] enable conductive morphology for cardiomyocytes maturation, and promote higher levels of cardiac markers, resulting in the construction of functional engineered cardiac tissues to be more like ventricular myocyte phenotypes. Examination of the expression of integrin receptors and a panel of transcripts linked to mechanotransduction revealed that the cardiac cells anchored onto CNT-GelMA through $\alpha 1\beta 1$ and $\alpha 2\beta 1$ integrins could be potentially matured through YAP/TAZ activation, unlike the cells on other hybrid scaffolds including rGO-GelMA. This work suggests that cardiomyocytes cultured on different hybrid scaffolds have distinct susceptibilities to extracellular guidance for functional maturation, which underlines the importance of model systems for cardiac tissue engineering, where high fidelity of cardiomyocyte phenotypes is desired.

EXPERIMENTAL METHODS

Materials.

Carboxyl-functionalized multiwalled carbon nanotubes were procured from NanoLab Inc. with a purity of 95%, diameter of 30 ± 15 nm, and length of 5 ± 20 μm. Gelatin (type A), methacrylic anhydride, 3-(trimethoxysilyl)propyl methacrylate (TMSPMA), L-ascorbic acid 2-phosphate sesquimagnesium salt hydrate, and blebbistatin were purchased from Sigma-Aldrich. 2-Hydroxy-1-(4-(hydroxyethoxy)phenyl)-2-methyl-1-propanone (Irgacure 2959) was obtained from CIBA Chemicals. The BCA Protein Assay Kit was acquired from ThermoFisher.

Synthesis of GelMA.

GelMA was prepared by following a previously reported protocol.[55] Briefly, a 10% (w/v) gelatin solution was prepared in Dulbecco's phosphate buffered saline (DPBS) and heated to 50° C. Methacrylic anhydride (0.8 mL per g of gelatin) was added dropwise to this gelatin solution and was allowed to react for 2 h under constant stirring at 50 °C. Subsequently, this reaction was stopped by adding four parts of DPBS to one part of the gelatin mixture. The product was subjected to dialysis using a Spectraphor dialysis membrane with a molecular weight cutoff of 12–14 kDa against deionized water (DW) at 40 °C for 5 days, followed by freeze-drying for 5 days before use.

Synthesis of GO and rGO.

GO was synthesized from graphite using a modified Hummers method.[64] In brief, concentrated H2SO4 containing 1.3% (w/v) of graphite powder (1 g), 1% (w/v) of sodium nitrate (NaNO3), and 4% (w/v) of potassium permanganate (KMnO4) was vigorously stirred at room temperature (RT) for 7 days. Subsequently, the reaction mixture was diluted by introducing eight parts of 5% aqueous H2SO4 to three parts of the reaction mixture, which was further stirred at 98 °C for 2 h. Afterward, the temperature was reduced to 60 °C, and 6 mL of 30% H2O2 solution was added to 275 mL of the reaction mixture. After stirring for 2 h, the mixture was centrifuged, and the solid pellet was collected. The product was washed 15 times with a solution containing 5% H2SO4 and 0.5% H2O2, followed by washing five times with 5% HCl solution. Finally, the pellet was repeatedly washed with DW until the pH of the supernatant became neutral. This material was then dried to obtain a brown powder. XPS measurements were performed on these nanoparticles using a Thermo Scientific

ESCALAB 250Xi XPS spectrometer with an electron flood gun operating at 0.2 mA (monochromatic Al Kα radiation, 1486.6 eV, 150W). Peak deconvolution of the C 1s spectra and atomic percentages from the survey spectra were determined using CasaXPS.

To synthesize rGO nanoparticles, the GO solution from the above step was reduced using ascorbic acid (100 mM). This reaction mixture was then sonicated (Crest Ultrasonics, model no. 275DA, USA) for 60 min. Subsequently, the solution was incubated at 80 °C for 48 h to accelerate the reduction process. Then, product was dialyzed (membrane cutoff: 12–14 kDa) against DW for 5 days at 40 °C, followed by drying the dialyzed product at 80 °C.

Preparation and Characterization of Nanoparticle Dispersions.

CNT, GO, and rGO nanoparticles were individually dispersed at a concentration of 0.5% (w/v) in DW containing 3.5% (w/v) GelMA, through sonication (2 s ON and 1 s OFF for 1 h, 80 W, VCX Sonics, USA). Morphological traits of the GelMA-coated CNT dispersion were characterized using a high-resolution TEM (Tecnai 12, FEI) with uranyl acetate stained, holey carbon film-supported grids. GelMA-coated GO and rGO dispersions, on the other hand, were analyzed using AFM (Multimode IV, Veeco, USA). Both dispersions were washed three time with DPBS by centrifugation at 14 000 rpm for 30 min to remove excess gelatin. 3-Aminopropyl trimethoxysilane-coated SiO_2 substrates were then utilized to load the samples. Surface topography of the nanoparticle dispersions was also obtained through AFM (Asylum Research, model MFP-3D), albeit following a different approach for sample preparation and analysis. The nanoparticle dispersions were spin-coated onto coverslips and mapped at a resonance frequency of 13 kHz, using a probe (Veeco Probes, Camarillo, CA, USA, SPM-PIC) with a spring constant of 0.2 N m^{-1}. To assess sheet resistance of CBNs, a GO nanoparticle dispersion (0.5% (w/v)) was added into the polydimethylsiloxane (PDMS) mold (~10 mm diameter) that has a glass bottom. CNT and rGO nanoparticles were individually dispersed at a concentration of0.5% (w/v) in ethanol through sonication, and then the CNT and rGO dispersed solutions were individually poured into the PDMS mold to obtain CBN films (~10 μm). For the GelMA film, 7% (w/v) GeMA prepolymer solution was poured into the mold and then dried. The sheet resistance of CNTs, rGO, GO, and pure GelMA films were measured by the four-point probe detection method with a Keithley 2400.

Formation and Characterization of Nanoparticle-Incorporated Hydrogel Thin Films.

Nanoparticle dispersions were diluted to 0.3% (w/v) with DPBS containing GelMA and Irgacure 2959 such that their final concentrations were 7% (w/v) and 0.5% (w/v), respectively. These hydrogel precursor solutions were then utilized to fabricate 50 μm thick hydrogel films on TMSPMA-coated 1.2 cm × 1.2 cm glass slides through UV cross-linking. The UV source was maintained at 8 cm from the target and tuned to an intensity of 7.64 mW cm^{-2}. CNT, GO, and rGO laden prepolymer solutions were cross-linked for 50, 3.5, and 65 s, respectively, to obtain substrates with similar elastic moduli. SEM (FEI/Philips XL30 FEG SEM) was then utilized to image the synthesized hydrogels. For this purpose, the hydrogels were snap-frozen in liquid nitrogen, lyophilized, mounted onto aluminum holders and sputter-coated with gold. The bulk elastic modulus of the hydrogels was measured through nanoindentation (Nano-UTM) using a spherical indenter (1 mm in radius). All tests were carried out with a maximum load of 0.3 mN at an approach rate of 0.1 μm/s.

Subsequently, the Hertzian model for an elastic half-space with a rigid spherical indenter was utilized to calculate the elastic modulus. The applied load and the displacement are calculated as follows:

$$F = \frac{4}{3}E^*\sqrt{R}h^{3/2} \text{ and } \frac{1}{E^*} = \frac{1-\vartheta_1^2}{E_1} + \frac{1-\vartheta_2^2}{E_2}$$

where F is the applied load, R is the radius of the indenter, h is the indentation depth, E* is the effective elastic modulus, and E_2 and E_1 and ϑ_2 and ϑ_1 are the elastic modulus and Poisson ratio of the indenter and the samples, respectively.

Local elastic moduli of the hydrogels in DPBS were recorded using AFM (Bruker Dimension ICON) in a “PeakForce–quantitative nanomechanical property mapping” mode. A cantilever equipped with a nitride tip (0.5–0.7 μm in radius) at a resonance frequency of 120–180 kHz and spring constant of 0.7 N/m was used for the fluid imaging probe (Scanasyst-Fluid). Images were evaluated using Nanoscope Analysis offline software. Changes to protein adsorption onto the hydrogel surfaces with respect to the incorporated nanoparticles were determined using the BCA assay kit. For this purpose, the hydrogel thin films were incubated with 10% FBS for 24 h at 37 °C, followed by washing three times with DPBS to remove the residual FBS. The samples were then treated with 2% (w/v) sodium dodecyl sulfate in DW for6hat37 °C while continuously shaking at 50 rpm. The supernatant was processed according to the manufacturer’s protocol.

Cell Isolation and Culture.

All animal protocols employed in this work were approved by the Institute’s Committee on Animal Care. Neonatal cardiomyocytes were isolated from 2-day-old Sprague–Dawley rats through collagenase-based enzymatic digestion. As we previously reported, the estimated ratio of isolated CMs and CFs was around 77.3% and 22.7%, respectively.[65] In brief, hearts extracted from the neonatal rats were washed thoroughly in Hank’s balanced salt solution and incubated overnight with trypsin at 4 °C. Next, the tissues were subjected to collagenase type II at 37 °C for digestion, and the extracted cardiomyocytes were enriched by preplating for 2 h. The isolated cells were then seeded onto different hybrid hydrogel substrates at a density of 0.375×10^5 cells/cm^2 unless stated otherwise. Culture conditions included Dulbecco’s modified Eagle medium (Gibco, USA) containing 10% (v/v) FBS (Gibco, USA), 1% (v/v) L-glutamine (Gibco, USA), and 100 μg/mL penicillin–streptomycin (Gibco, USA). The serum concentration was reduced to 2% (v/v) after 2 days in culture to limit the proliferation of cardiac fibroblasts. In certain instances, only cardiac fibroblasts were used, and, in such cases, cardiac fibroblasts were seeded at a density of 5×10^4 cells/cm^2 unless stated otherwise.

Characterization of Cellular Behavior.

At various time points, cellular (DNA) content on different substrates was assessed by the PicoGreen assay (Invitrogen). For this purpose, cells in DW were ruptured by treating them with a freeze–thawing cycle. The supernatant was then processed as per the manufacturer’s

protocol. On the other hand, proliferation of cardiac fibroblasts on various substrates was assessed by the MTS proliferation assay (Promega).

For all staining purposes, cells were fixed with 4% (w/v) paraformaldehyde in PBS for 10 min and washed three times with PBS. For staining F-actin and nucleus, Alexa Fluor 488 phalloidin and DAPI (ThermoFisher) were used. In cases of immunostaining, after fixation, cells were permeabilized with 0.1% (v/v) Triton-X100 in PBS and blocked with 10% goat serum in PBS. Cells were then treated overnight at 4 °C with primary antibodies: sarcomeric α-actinin and connexin 43 or troponin I (Abcam). Subsequently, they were washed three times with PBS with 10 min intervals and treated with corresponding secondary antibodies for 40 min at RT. Cells were again washed with PBS and counterstained with DAPI. Finally, they were imaged with an Olympus inverted laser scanning confocal microscope. Images were then quantified with CellProfiler software (cell area, eccentricity, and Cx43 expression) and ImageJ (vinculin and troponin I expression). MATLAB was used for profiling sarcomeric α-actinin. Single-cell images were uploaded to Cell-Profiler software, and their boundaries were determined using the “identify primary objects” module. Once the boundaries were defined, cell area, form factor, eccentricity, and aspect ratio were derived using the “measure object size shape” module. All the immunofluorescent quantifications were performed with individual cells, and then the intensities were averaged and normalized.

Electrophysiological Assessment.

Beating patterns of cardiomyocytes in different substrates were recorded daily using a Zeiss microscope equipped with a temperature-controlled chamber. The videos were then processed with MATLAB as previously described to extract beating frequency of cardiomyocytes on various substrates.[16] The response of cells to an external electric field was tested using an electrical pulse generator (pulse/function generator 50 MHz, Hewlett-Packard). The excitation threshold for each substrate was calculated at the frequencies 0.5, 1, 2, and 3 Hz.[16,17]

Whole cell current clamp recordings were conducted with an Axopatch 200A amplifier. Electrical signals were recorded using a Digidata 1440A data acquisition system controlled by pCLAMP10 software (Molecular Devices). Borosilicate glass pipets pulled using a P-97 puller (Sutter Instruments) with a resistance 2–3 MΩ were used. The external solution was made up of 140 mM NaCl, 5 mM KCl, 2 mM $CaCl_2$, 2 mM $MgCl_2$, 10 mM HEPES, and 10 mM D-glucose and adjusted to a pH of 7.4 with NaOH (Boston BioProducts). The pipet internal solution was made up of 5 mM NaCl, 140 mM KCl, 0.5 mM $CaCl_2$, 2 mM $MgCl_2$, 5 mM EGTA, 10 mM HEPES, and 3 mM Na_2ATP and adjusted to a pH of 7.2 with NaOH. Cell membrane capacitance was compensated after establishing whole-cell recordings, and spontaneous firings were recorded in a gap-free mode. The data analysis was conducted using Clampfit 10 (Molecular Devices). Upstroke velocity (($V_p - V_0$/($T_p - T_0$)) and action potential period evaluated at 50% (APD50 = $T_{p50} - T_0$) and 90% (APD90 = $T_{p90} - T_0$) of repolarization were calculated as shown in Figure S6 and follow a previously established method.[66]

Blebbistatin Treatment.

Cardiomyocytes were seeded and allowed to attach on the hybrid scaffolds for 24 h. Then blebbistatin was supplemented in the media at 1 μM for 24 h (24–48 h) and removed for the next 24 h (48–72 h), and this cycle was repeated once more (exposure: 72–96 h and removal: 96–120 h). Phase-contrast images were acquired daily using a Zeiss microscope, and the images were quantified using ImageJ software.

RNA Isolation and qRT-PCR.

TRIzol and SuperScript III First-Strand Synthesis SuperMix (Invitrogen) were used for RNA extraction and cDNA synthesis, respectively. qRT-PCR analyses were then carried out with SYBR Green Master Mix in an IQ5 detection system (Biorad). Expression levels of mRNA in all samples were quantified based on relative cycle numbers to the internal control, glyceraldehyde-3-phosphate dehydrogenase. All primers used in this work have been listed in the Supporting Information (Table S1).

Statistical Analysis.

Error bars represent the mean ± standard deviation (SD). Student's t test, one-way Anova, two-way Anova, Kruskal–Wallis test, and the D'Agostino and Pearson normality test were performed wherever necessary (Graphpad Prism 7). $P < 0.05$ was considered statistically significant for all statistical tests.

Supplementary Material

Refer to Web version on PubMed Central for supplementary material.

ACKNOWLEDGMENTS

The authors gratefully acknowledge funding by the National Institutes of Health (R01AR074234 and R21EB026824). S.R.S. would like to recognize and thank Brigham and Women's Hospital President Betsy Nabel, MD, and the Reny family, for the Stepping Strong Innovator Award through their generous funding. M.A.H. thanks the support of the NSTIP strategic technologies program in the Kingdom of Saudi Arabia, award no. 11-NAN1544-03. A discovery grant to X.T. from the Natural Sciences and Engineering Research Council (NSERC) of Canada is acknowledged. S.M. and B.B.M. would like to thank the Fulbright Nehru Doctoral Fellowship and Department of Biotechnology, Govt. of India, for their respective funding.

REFERENCES

(1). Souders CA; Bowers SL; Baudino TA Cardiac Fibroblast: The Renaissance Cell. Circ. Res 2009, 105, 1164–1176. [PubMed: 19959782]

(2). Banerjee I; Fuseler JW; Price RL; Borg TK; Baudino TA Determination of Cell Types and Numbers during Cardiac Development in the Neonatal and Adult Rat and Mouse. Am. J. Physiol. Heart Circ. Physiol 2007, 293, H1883–H1891. [PubMed: 17604329]

(3). Woodcock EA; Matkovich SJ Cardiomyocytes Structure, Function and Associated Pathologies. Int.J. Biochem. Cell Biol 2005, 37, 1746–1751. [PubMed: 15950518]

(4). Pfeiffer ER; Tangney JR; Omens JH; McCulloch AD Biomechanics of Cardiac Electromechanical Coupling and Mechano-electric Feedback. J. Biomech. Eng 2014, 136, 021007. [PubMed: 24337452]

(5). Kikuchi K; Poss KD Cardiac Regenerative Capacity and Mechanisms. Annu. Rev. Cell Dev. Biol 2012, 28, 719–741. [PubMed: 23057748]

(6). Foglia MJ; Poss KD Building and Re-Building the Heart by Cardiomyocyte Proliferation. Development 2016, 143, 729–740. [PubMed: 26932668]

(7). Chiu LLY; Radisic M Cardiac Tissue Engineering. Curr. Opin. Chem. Eng 2013, 2, 41–52.

(8). Scuderi GJ; Butcher J Naturally Engineered Maturation of Cardiomyocytes. Front. Cell Dev. Biol 2017, 5, 50. [PubMed: 28529939]

(9). Engler AJ; Carag-krieger C; Johnson CP; Raab M; Tang H; Speicher DW; Sanger JW; Sanger JM; Discher DE Embryonic Cardiomyocytes Beat Best on a Matrix with Heart-like Elasticity : Scarlike Rigidity Inhibits Beating. J. Cell Sci 2008, 121, 3794–3802. [PubMed: 18957515]

(10). Chang W-T; Yu D; Lai Y-C; Lin K-Y; Liau I Characterization of the Mechanodynamic Response of Cardiomyocytes with Atomic Force Microscopy. Anal. Chem 2013, 85, 1395–1400. [PubMed: 23265281]

(11). Martins AM; Eng G; Caridade SG; Mano JF; Reis RL; Vunjak-Novakovic G Electrically Conductive Chitosan/Carbon Scaffolds for Cardiac Tissue Engineering. Biomacromolecules 2014, 15, 635–643. [PubMed: 24417502]

(12). Shin SR; Farzad R; Tamayol A; Manoharan V; Mostafalu P; Zhang YS; Akbari M; Jung SM; Kim D; Comotto M; Annabi N; Al-Hazmi FE; Dokmeci MR; Khademhosseini A. A Bioactive Carbon Nanotube-Based Ink for Printing 2D and 3D Flexible Electronics. Adv. Mater 2016, 28, 3280–3289. [PubMed: 26915715]

(13). Pok S; Vitale F; Eichmann SL; Benavides OM; Pasquali M; Jacot JG Biocompatible Carbon Nanotube-Chitosan Scaffold Matching the Electrical Conductivity of the Heart. ACS Nano 2014, 8, 9822–9832. [PubMed: 25233037]

(14). Shin SR; Bae H; Cha JM; Mun JY; Chen Y-C; Tekin H; Shin H; Farshchi S; Dokmeci MR; Tang XS; Khademhosseini A. Carbon Nanotube Reinforced Hybrid Microgels as Scaffold Materials for Cell Encapsulation. ACS Nano 2012, 6, 362–372. [PubMed: 22117858]

(15). Kharaziha M; Shin SR; Nikkhah M; Topkaya SN; Masoumi N; Annabi N; Dokmeci MR; Khademhosseini A. Tough and Flexible CNT-Polymeric Hybrid Scaffolds for Engineering Cardiac Constructs. Biomaterials 2014, 35, 7346–7354. [PubMed: 24927679]

(16). Shin SR; Jung SM; Zalabany M; Kim K; Zorlutuna P; Kim SB; Nikkhah M; Khabiry M; Azize M; Kong J; Wan KT; Palacios T; Dokmeci MR; Bae H; Tang XS; Khademhosseini A. Carbon-Nanotube-Embedded Hydrogel Sheets for Engineering Cardiac Constructs and Bioactuators. ACS Nano 2013, 7, 2369–2380. [PubMed: 23363247]

(17). Shin SR; Zihlmann C; Akbari M; Assawes P; Cheung L; Zhang K; Manoharan V; Zhang YS; Yuksekkaya M; Wan K; Nikkhah M; Dokmeci MR; Tang XS; Khademhosseini A Reduced Graphene Oxide-GelMA Hybrid Hydrogels as Scaffolds for Cardiac Tissue Engineering. Small 2016, 12, 3677–3689. [PubMed: 27254107]

(18). Shin SR; Aghaei-ghareh-bolagh B; Dang TT; Topkaya SN; Gao X; Yang SY; Jung SM; Oh JH; Dokmeci MR; Tang XS; Khademhosseini A Cell-Laden Microengineered and Mechanically Tunable Hybrid Hydrogels of Gelatin and Graphene Oxide. Adv. Mater 2013, 25, 6385–6391. [PubMed: 23996513]

(19). Cha C; Shin SR; Gao X; Annabi N; Dokmeci MR; Tang XS; Khademhosseini A Controlling Mechanical Properties of Cell-Laden Hydrogels by Covalent Incorporation of Graphene Oxide. Small 2014, 10, 514–523. [PubMed: 24127350]

(20). Saravanan S; Sareen N; Abu-El-Rub E; Ashour H; Ashour H; Sequiera GL; Ammar HI; Gopinath V; Shamaa AA; Sayed SSE; Moudgil M; Vadivelu J; Dhingra S Graphene Oxide-Gold Nanosheets Containing Chitosan Scaffold Improves Ventricular Contractility and Function After Implantation into Infarcted Heart. Sci. Rep 2018, 8, 15069. [PubMed: 30305684]

(21). Zhou J; Yang X; Liu W; Wang C; Shen Y; Zhang F; Zhu H; Sun H; Chen J; Lam J; Mikos AG; Wang C Injectable OPF/Graphene Oxide Hydrogels Provide Mechanical Support and Enhance Cell Electrical Signaling after Implantation into Myocardial Infarct. Theranostics 2018, 8, 3317–3330. [PubMed: 29930732]

(22). Liu H; Cheng J; Chen F; Hou F; Bai D; Xi P; Zeng Z Biomimetic and Cell-Mediated Mineralization of Hydroxyapatite by Carrageenan Functionalized Graphene Oxide. ACS Appl. Mater. Interfaces 2014, 6, 3132–3140. [PubMed: 24527702]

(23). Dvir T; Timko BP; Brigham MD; Naik SR; Karajanagi SS; Levy O; Jin H; Parker KK; Langer R; Kohane DS Nanowired Three-Dimensional Cardiac Patches. Nat. Nanotechnol 2011, 6, 720–725. [PubMed: 21946708]

(24). Navaei A; Saini H; Christenson W; Christenson W; Sullivan RT; Ros R; Nikkhah M. Gold Nanorod-Incorporated Gelatin-Based Conductive Hydrogels for Engineering Cardiac Tissue Constructs. Acta Biomater. 2016, 41, 133–146. [PubMed: 27212425]

(25). Shevach M.; Fleischer S.; Shapira A.; Dvir T. Gold Nanoparticle-Decellularized Matrix Hybrids for Cardiac Tissue Engineering. Nano Lett. 2014, 14, 5792–5796. [PubMed: 25176294]

(26). Fleischer S; Shevach M; Feiner R; Dvir T Coiled Fiber Scaffolds Embedded with Gold Nanoparticles Improve the Performance of Engineered Cardiac Tissues. Nanoscale 2014, 6, 9410–9414. [PubMed: 24744098]

(27). Ravichandran R; Sridhar R; Venugopal JR; Sundarrajan S; Mukherjee S; Ramakrishna S Gold Nanoparticle Loaded Hybrid Nanofibers for Cardiogenic Differentiation of Stem Cells for Infarcted Myocardium Regeneration. Macromol Biosci. 2014, 14, 515–525. [PubMed: 24327549]

(28). Shin SR; Li Y-C; Jang HL; Khoshakhlagh P; Akbari M; Nasajpour A; Zhang YS; Tamayol A; Khademhosseini A Graphene-Based Materials for Tissue Engineering. Adv. Drug Delivery Rev 2016, 105, 255–274.

(29). Annabi N; Shin SR; Tamayol A; Miscuglio M; Bakooshli MA; Assmann A; Mostafalu P; Sun J; Mithieux S; Cheung L; Tang XS; Weiss AS; Khademhosseini A Highly Elastic and Conductive Human-Based Protein Hybrid Hydrogels. Adv. Mater 2016, 28, 40–49. [PubMed: 26551969]

(30). Shin SR; Aghaei-ghareh-bolagh B; Gao X; Nikkhah M; Jung SM; Dolatshahi-pirouz A; Kim SB; Kim SM; Dokmeci MR; Tang XS; Khademhosseini A Layer-by-Layer Assembly of 3D Tissue Constructs with Functionalized Graphene. Adv. Funct. Mater 2014, 24, 6136–6144. [PubMed: 25419209]

(31). Sayyar S; Murray E; Thompson BC; Chung J; Officer DL; Gambhir S; Spinks GM; Wallace GG Processable Conducting Graphene/Chitosan Hydrogels for Tissue Engineering. J. Mater. Chem. B 2015, 3, 481–490.

(32). Samarel AM Costameres, Focal Adhesions, and Cardiomyocyte Mechanotransduction. Am. J. Physiol. Hear. Circ. Physiol 2005, 289, H2291–H2301.

(33). Lammerding J; Kamm RD; Lee RT Mechanotransduction in Cardiac Myocytes. Ann. N. Y. Acad. Sci 2004, 1015, 53–70. [PubMed: 15201149]

(34). Morikawa Y; Zhang M; Heallen T; Leach J; Tao G; Xiao Y; Bai Y; Li W; Willerson JT; Martin JF Actin Cytoskeletal Remodeling with Protrusion Formation Is Essential for Heart Regeneration in Hippo-Deficient Mice. Sci. Signaling 2015, 8, ra41.

(35). Mosqueira D; Pagliari S; Uto K; Ebara M; Romanazzo S; Escobedo-lucea C; Nakanishi J; Taniguchi A; Franzese O; Di Nardo P; Goumans MJ; Traversa E; Pinto-do-O P; Aoyagi T; Forte G Hippo Pathway Effectors Control Cardiac Progenitor Cell Fate by Acting as Dynamic Sensors of Substrate Mechanics and Nanostructure. ACS Nano 2014, 8, 2033–2047. [PubMed: 24483337]

(36). Xin M; Kim Y; Sutherland LB; Murakami M; Qi X; McAnally J; Porrello ER; Mahmoud A; Tan W; Shelton JM; Richardson JA; Sadek HA; Bassel-Duby R; Olson EN Hippo Pathway Effector Yap Promotes Cardiac Regeneration. Proc. Natl. Acad. Sci. U. S. A 2013, 110, 13839–13844. [PubMed: 23918388]

(37). Gise VA; Lin Z; Schlegelmilch K; Honor LB; Pan GM; Buck JN; Ma Q; Ishiwata T; Zhou B; Carmargo FD; Pu WT YAP1, the Nuclear Target of Hippo Signaling, Stimulates Heart Growth through Cardiomyocyte Proliferation but Not Hypertrophy. Proc. Natl. Acad. Sci. U. S. A 2012, 109, 2394–2399. [PubMed: 22308401]

(38). Okpalugo TIT; Papakonstantinou P; Murphy H; Mclaughlin J; Brown NMD. High Resolution XPS Characterization of Chemical Functionalised MWCNTs and SWCNTs. Carbon 2005, 43, 153–161.

(39). Yeung T; Georges PC; Flanagan LA; Marg B; Ortiz M; Funaki M; Zahir N; Ming W; Weaver V; Janmey PA Effects of Substrate Stiffness on Cell Morphology, Cytoskeletal Structure, and Adhesion. Cell Motil Cytoskeleton 2005, 60, 24–34. [PubMed: 15573414]

(40). Schrader J; Gordon-Walker TT; Aucott RL; van Deemeter M; Quaas A; Walsh S; Benten D; Forbes SJ; Wells RG; Iredale JP. Matrix Stiffness Modulates Proliferation, Chemotherapeutic Response, and Dormancy in Hepatocellular Carcinoma Cells. Hepatology 2011, 53, 1192–1205. [PubMed: 21442631]

(41). Engler AJ; Sen S; Sweeney HL; Discher DE Matrix Elasticity Directs Stem Cell Lineage Specification. Cell 2006,126,677–689. [PubMed: 16923388]

(42). Lee J; Abdeen AA; Zhang D; Kilian KA Directing Stem Cell Fate on Hydrogel Substrates by Controlling Cell Geometry, Matrix Mechanics and Adhesion Ligand Composition. Biomaterials 2013, 34, 8140–8148. [PubMed: 23932245]

(43). Ribeiro AJ; Ang YS; Fu JD; Rivas RN; Mohamed TM; Higgs GC; Srivastava D; Pruitt BL Contractility of Single Cardiomyocytes Differentiated from Pluripotent Stem Cells Depends on Physiological Shape and Substrate Stiffness. Proc. Natl. Acad. Sci. U. S. A 2015, 112, 12705–12710. [PubMed: 26417073]

(44). Hlady V; Buijs J Protein Adsorption on Solid Surfaces. Curr. Opin. Biotechnol 1996, 7, 72–77. [PubMed: 8791316]

(45). Yu J; Kan Y; Rapp M; Danner E; Wei W; Das S; Miller DR; Chen Y; Waite JH; Israelachvili JN Adaptive Hydrophobic and Hydrophilic Interactions of Mussel Foot Proteins with Organic Thin Films. Proc. Natl. Acad. Sci. U. S. A 2013, 110, 15680–15685. [PubMed: 24014592]

(46). Rechendorff K; Hovgaard MB; Foss M; Zhdanov VP; Besenbacher F Enhancement of Protein Adsorption Induced by Surface Roughness. Langmuir 2006, 22, 10885–10888. [PubMed: 17154557]

(47). Shemesh T; Geiger B; Bershadsky AD; Kozlov MM Focal Adhesions as Mechanosensors: A Physical Mechanism. Proc. Natl. Acad. Sci. U. S. A 2005, 102, 12383–12388. [PubMed: 16113084]

(48). Fearnley CJ; Roderick HL; Bootman MD Calcium Signaling in Cardiac Myocytes. Cold Spring Harbor Perspect. Biol 2011, 3, a004242.

(49). Muller M; Fleishmann BK; Selbert S; Ji GJ; Endl E; Middeler G; Muller OJ; Schlenke P; Frese S; Wobus AM; Hescheler J; Katus HA; Franz WM Selection of Ventricular-like Cardiomyocytes from ES Cells in Vitro. FASEB J. 2000,14,2540–2548. [PubMed: 11099473]

(50). Bartos DC; Grandi E; Ripplinger CM Ion Channels in the Heart. Compr. Physiol 2015, 5, 1423–1464. [PubMed: 26140724]

(51). Tamargo J; Caballero R; Gomez R; Valenzuela C; Delpo E Pharmacology of Cardiac Potassium Channels. Cardiovasc. Res 2004, 62, 9–33. [PubMed: 15023549]

(52). Benito B; Josephson ME Ventricular Tachycardia in Coronary Artery Disease. Rev. Esp. Cardiol 2012, 65, 939–955. [PubMed: 22951088]

(53). Skwarek-maruszewska A; Hotulainen P; Mattila PK; Lappalainen P Contractility-Dependent Actin Dynamics in Cardiomyocyte Sarcomeres. J. Cell Sci 2009, 122, 2119–2126. [PubMed: 19470580]

(54). Humphries JD; Byron A; Humphries MJ Integrin Ligands at a Glance. J. Cell Sci 2006, 119, 3901–3903. [PubMed: 16988024]

(55). Nichol JW; Koshy ST; Bae H; Hwang CM; Yamanlar S; Khademhosseini A Cell-Laden Microengineered Gelatin Methacrylate Hydrogels. Biomaterials 2010, 31, 5536–5544. [PubMed: 20417964]

(56). Heino J Cellular Signaling by Collagen-Binding Integrins. Adv. Exp.Med. Biol 2014, 819, 143–155. [PubMed: 25023173]

(57). Li Y; Shi X; Tian L; Sun H; Wu Y; Li X; Li J; Wei Y; Han X; Zhang J; Jia X; Bai R; Jing L; Ding P; Liu H; Han D AuNP-Collagen Matrix with Localized Stiffness for Cardiac-Tissue Engineering: Enhancing the Assembly of Intercalated Discs by β1-Integrin-Mediated Signaling. Adv. Mater 2016, 28, 10230–10235. [PubMed: 27723133]

(58). Nardone G; Oliver-De La Cruz J; Vrbsky J; Martini C; Pribyl J; Skladal P; Pesl M; Caluori G; Pagliari S; Martino F; Maceckova Z; Hajduch M; Sanz-Garcia A; Pugno NM; Stokin GB; Forte G YAP Regulates Cell Mechanics by Controlling Focal Adhesion Assembly. Nat. Commun 2017, 8, 15321. [PubMed: 28504269]

(59). Lamar JM; Xiao Y; Norton E; Jiang ZG; Gerhard GM; Kooner S; Warren JSA; Hynes RO SRC Tyrosine Kinase Activate the YAP/TAZ Axis and thereby Drives Tumor Growth and Metastasis. J. Biol. Chem 2019, 294, 2302–2317. [PubMed: 30559289]

(60). Yu FX; Zhao B; Panupinthu N; Jewell JL; Lian I; Wang LH; Zhao J; Yuan H; Tumaneng K; Li H; Fu XD; Mills GB; Guan KL Regulation of the Hippo-YAP Pathway by G-Protein-Coupled Receptor Signaling. Cell 2012, 150, 780–791. [PubMed: 22863277]

(61). Feng X; Degese MS; Iglesias-bartolome R; Vaque JP; Molinolo AA; Rodrigues M; Zaidi MR; Ksander BR; Merlino G; Sodhi A; Chen Q; Gutkind JS Hippo-Independent Activation of YAP by the GNAQ Uveal Melanoma Oncogene through a Trio-Regulated Rho GTPase Signaling Circuitry. Cancer Cell 2014, 25, 831–845. [PubMed: 24882515]

(62). Brancaccio M; Guazzone S; Menini N; Sibona E; Hirsch E; De Andrea M; Rocchi M; Altruda F; Tarone G; Silengo L Melusin is a New Muscle-Specific Interactor for beta(1) Integrin Cytoplasmic Domain. J. Biol. Chem 1999, 274, 29282–29288. [PubMed: 10506186]

(63). Unsold B; Kaul A; Sbroggio M; Schubert C; Regitz-zagrosek V; Brancaccio M; Damilano F; Hirsch E; Van Bilsen M; Munts C; Sipido K; Bito V; Detre E; Wagner NM; Schöfer K; Seidler T; Vogt J; Neef S; Bleckmann A; Maier LS; et al. Melusin Protects from Cardiac Rupture and Improves Functional Remodelling after Myocardial Infarction. Cardiovasc. Res 2014, 101, 97–107. [PubMed: 24130190]

(64). Chen J; Yao B; Li C; Shi G An Improved Hummers Method for Eco-Friendly Synthesis of Graphene Oxide. Carbon 2013, 64, 225–229.

(65). Sadeghi AH; Shin SR; Deddens JC; Fratta G; Mandla S; Yazdi IK; Prakash G; Antona S; Demarchi D; Buijsrogge MP; Sluijter JPG; Hjortnaes J; Khademhosseini A Engineered 3D Cardiac Fibrotic Tissue to Study Fibrotic Remodeling. Adv. Healthcare Mater 2017, 6, 1601434.

(66). Strasburger JF; Wacker-Gussmann A Fetal and Neonatal Physiology Section XI: Fetal and Neonatal Cardiovascular Physiology; 51 - Developmental Electrophysiology in the Fetus and Neonate, 5th ed.; Elsevier, 2017; pp 522–539.

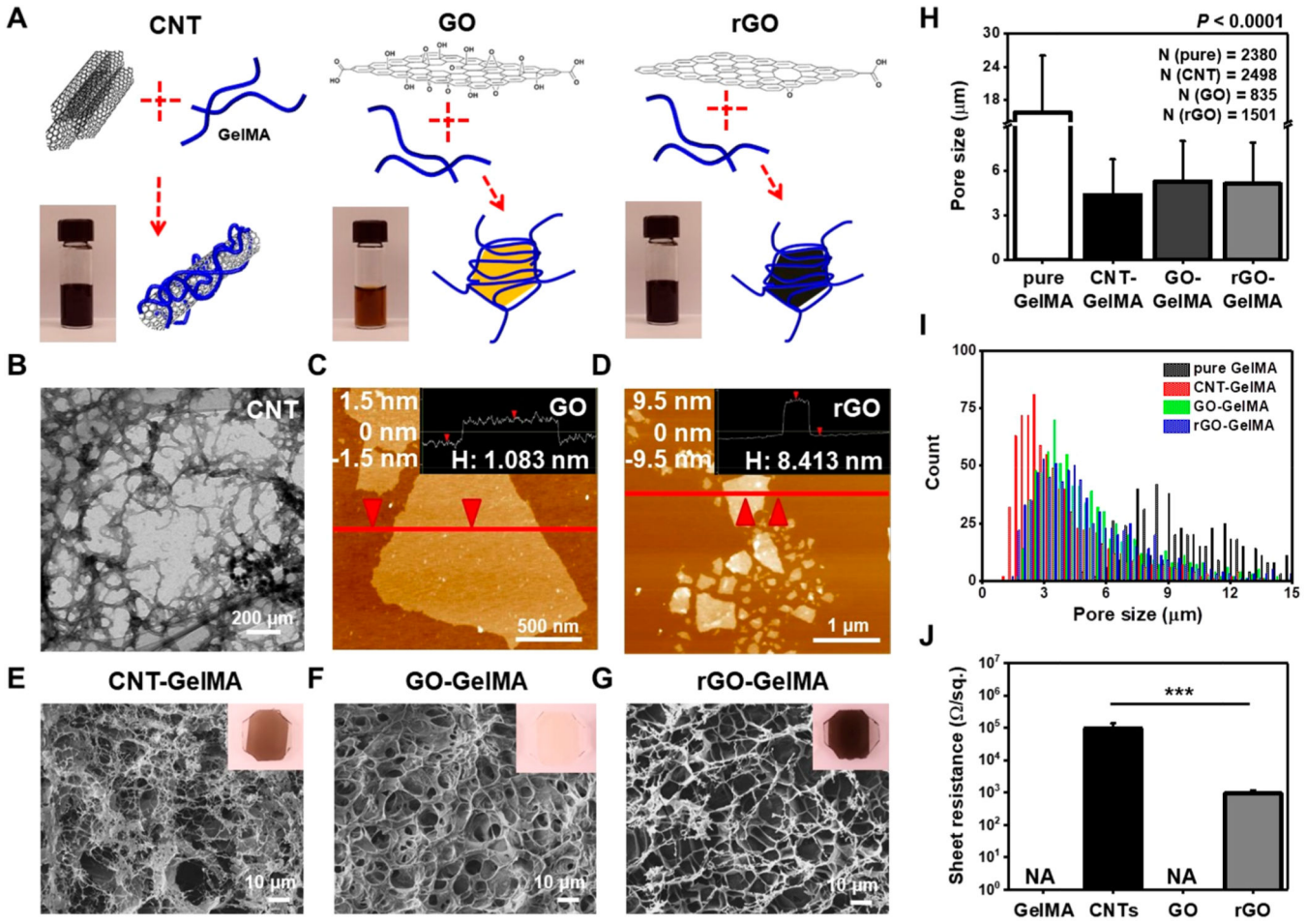

Figure 1.

Structural and electrical characteristics of CNT-, GO-, and rGO-GelMA. (A) Preparation procedure of CNT-, GO-, and rGO-GelMA hybrid hydrogels. (B) TEM image of CNTs. AFM images of (C) GO and (D) rGO. Inset images in (C) and (D) display the height profile along the specified line in each image. SEM images exhibiting porous surfaces of (E) CNT-, (F) GO-, and (G) rGO-GelMA thin films. Inset optical images in (E)-(G) display CNT-, GO-, and rGO-GelMA thin films on TMSPMA-treated glass slides, respectively. (H) Pore size analysis of pure, CNT-, GO-, and rGO-GelMA. (I) Histograms of the pore sizes of pure, CNT-, GO-, and rGO-GelMA. (J) Sheet resistance of CBNs, showing CNTs and rGO are conductive while pure GelMA and GO are nonconductive (N=3) (***P < 0.0005). Error bars represent standard deviation.

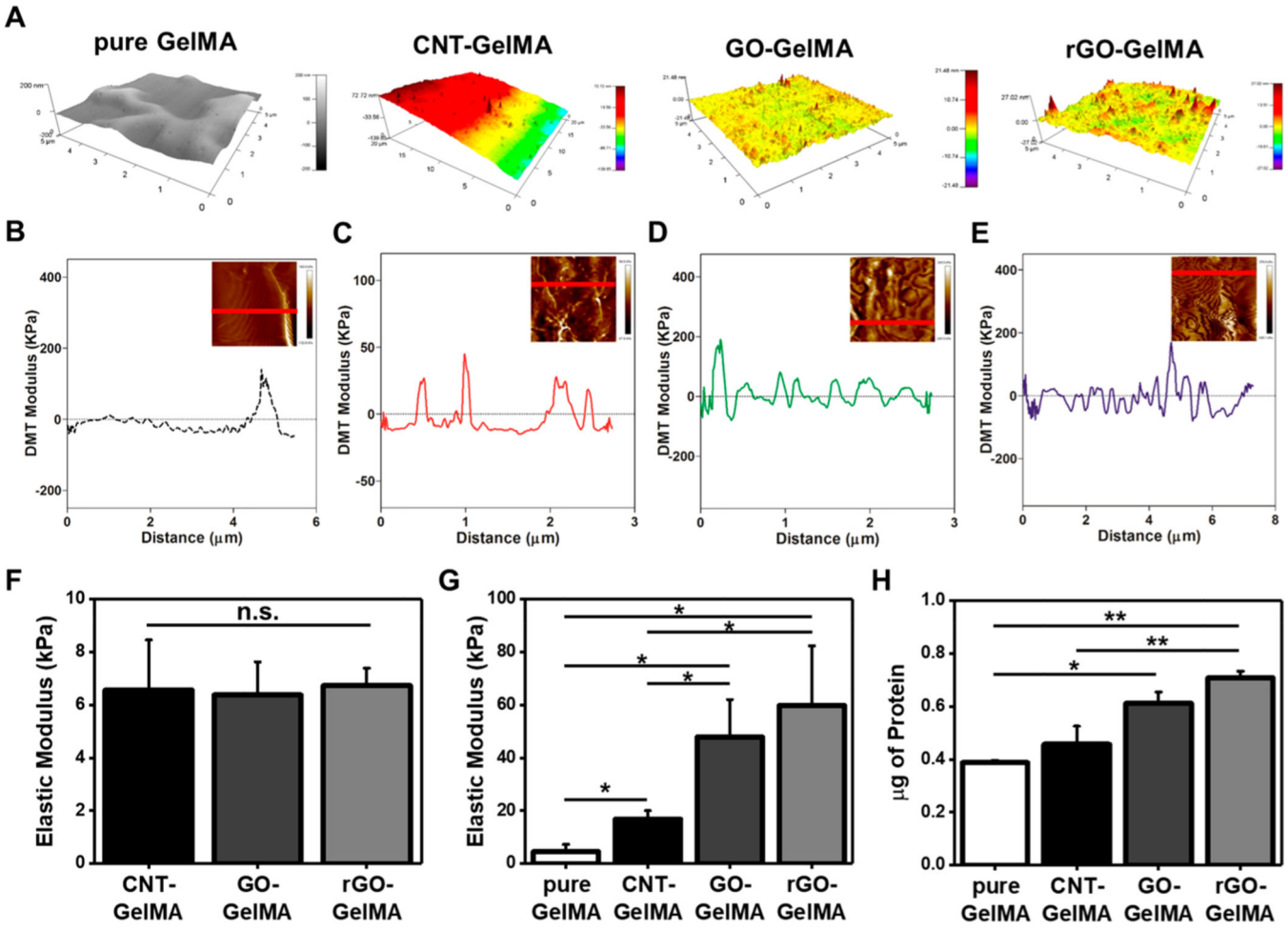

Figure 2.

Topological and mechanical characterizations of engineered hybrid hydrogels and protein adsorption onto their surface. (A) Spatial topography of pure, CNT-, GO-, and rGO-GelMA, measured by AFM. DMT modulus distribution profile of (B) pure, (C) CNT-, (d) GO-, and (E) rGO-GelMA along the specified line in inset AFM images of each condition. (F) Macroscale elastic modulus of CNT-, GO-, and rGO- GelMA ($N = 4$ for CNT, $N = 5$ for GO, $N = 4$ for rGO). (G) Local elastic modulus of pure, CNT-, GO-, and rGO-GelMA obtained from the force—deformation plots in (B)-(E) ($N = 3$). (H) Quantification of absorbed proteins on the surface of pure, CNT-, GO-, and rGO-GelMA ($N = 2$) (*$P < 0.05$, **$P < 0.005$). Error bars represent standard deviation.

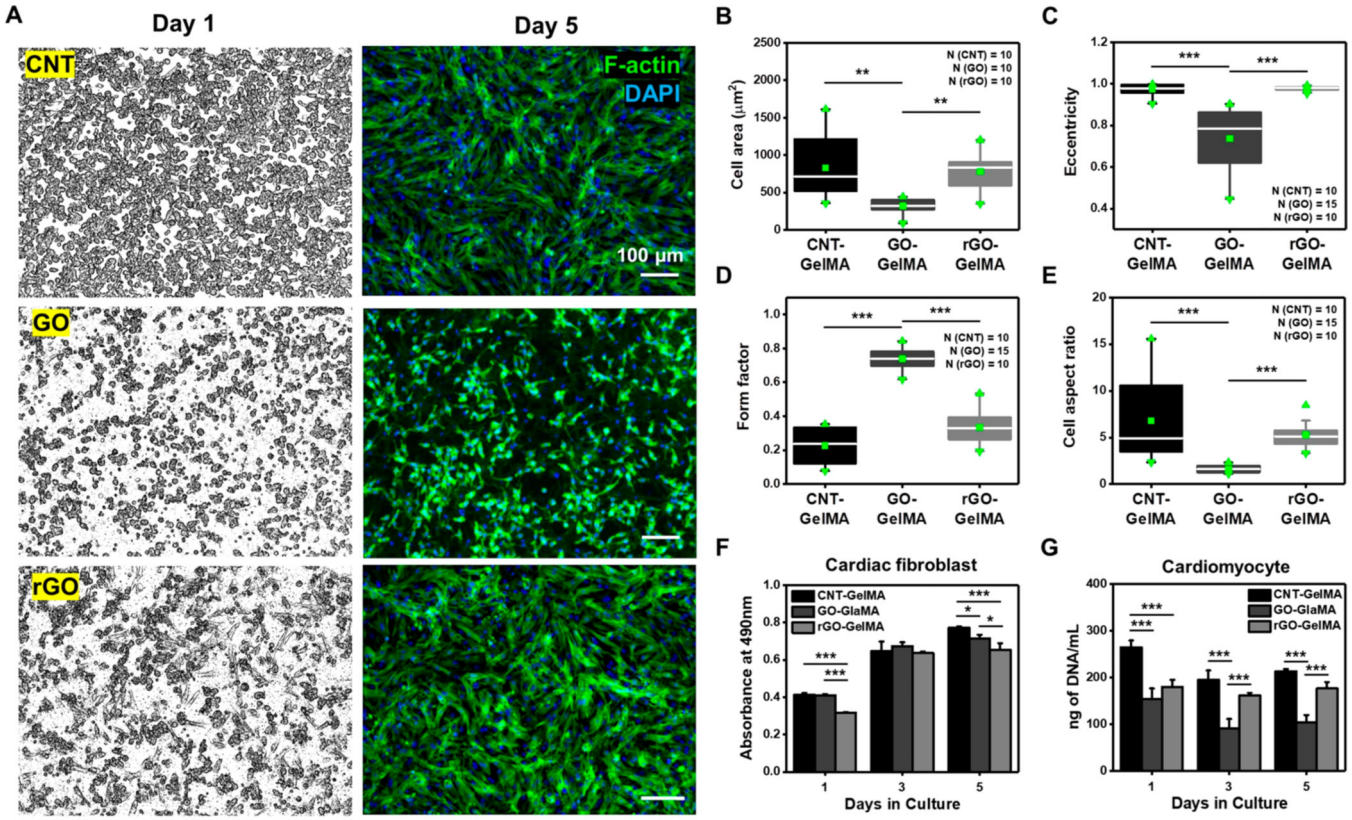

Figure 3.

Comparison of organization and proliferation for cardiomyocytes cultured on different hybrid scaffolds. (A) Immunofluorescence images of cardiomyocytes cultured for 1 and 5 days on CNT-, GO-, and rGO-GelMA. (B) Cell area, (C) eccentricity, (D) form factor, and (E) aspect ratio of cardiomyocytes cultured for 5 days on CNT-, GO-, and rGO-GelMA, displaying that the conductive scaffolds (CNT- and rGO-GelMA) promote better cardiac cell morphology of cardiomyocytes compared to nonconductive GO-GelMA. (F) MTT assay results for cardiac fibroblasts cultured on CNT-, GO-, and rGO-GelMA ($N = 4$). (G) DNA quantities on days 1, 3, and 5 showing higher levels of proliferative cardiomyocytes cultured on CNT-GelMA relative to those cultured on GO- and rGO-GelMA ($N = 4$) (*$P < 0.05$, **$P < 0.005$, ***$P < 0.005$). Error bars represent standard deviation.

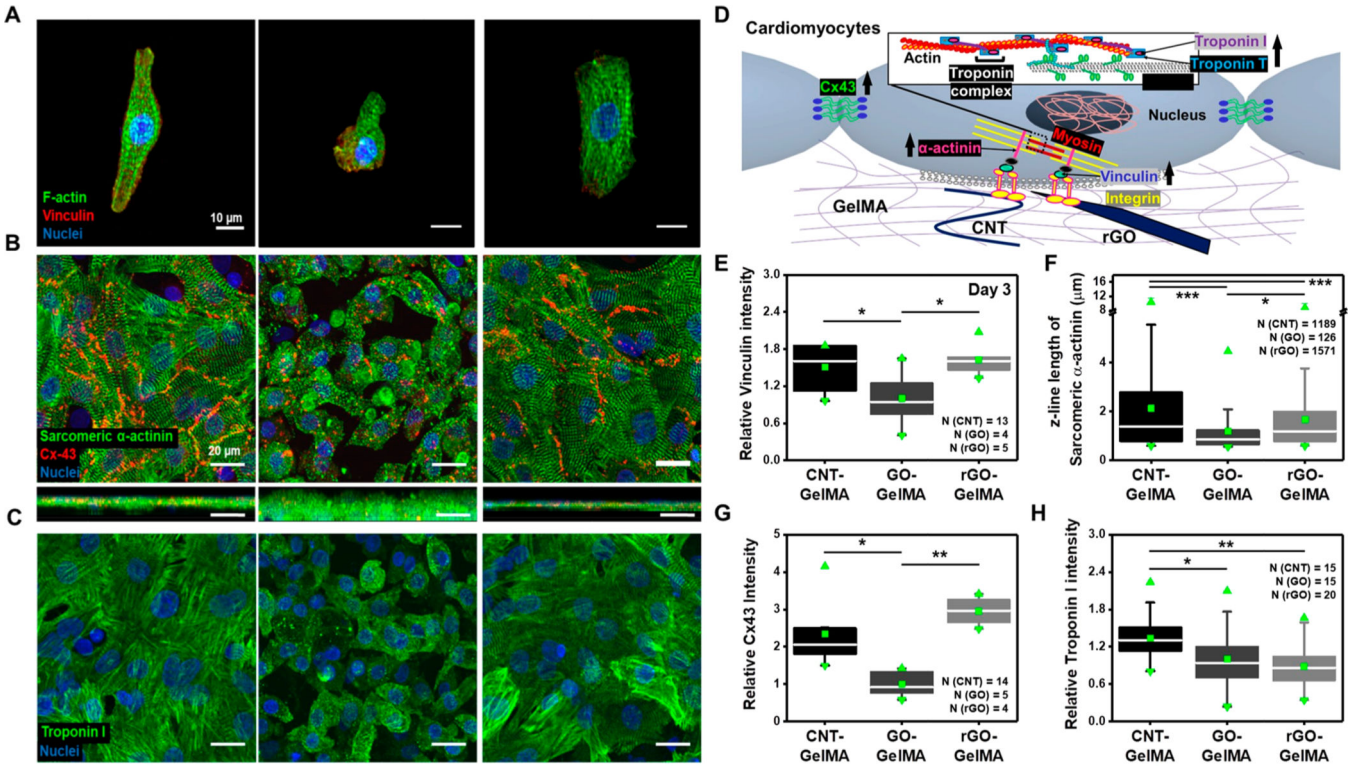

Figure 4.

Phenotypes of cardiac cells cultured on different hybrid scaffolds based on expression of cardiac specific markers. (A) Immunofluorescence images of cardiomyocytes cultured on CNT-, GO-, and rGO-GelMA stained for F-actin (green), vinculin (red), and nuclei (blue). (B) Immunostaining of sarcomeric α-actinin (green), Cx-43 (red), and nuclei (blue) showing cardiac tissues cultured for 5 days on CNT-, GO-, and rGO-GelMA are phenotypically different. Bottom images display cross-section images of cardiac tissues. (C) Immunofluorescence images of cardiomyocytes on CNT-, GO-, and rGO-GelMA stained for troponin I (green) and nuclei (blue). (D) Cartoon showing a schematic representation of part of important proteins for cardiomyocytes during maturation such as integrin (yellow), vinculin (royal), α-actinin (pink), myosin (red), troponin I (purple) and T (blue), and Cx43 (green). (E) Relative intensity of vinculin for cells cultured for 5 days on CNT-, GO-, and rGO-GelMA. (F) Z-line length of sarcomeric α-actinin of cardiomyocytes on different hybrid scaffolds on day 5. Relative intensity of (G) Cx43 and (H) troponin I for cells cultured for 5 days on CNT-, GO-, and rGO-GelMA (*$P < 0.05$, **$P < 0.005$, ***$P < 0.005$). Error bars represent standard deviation.

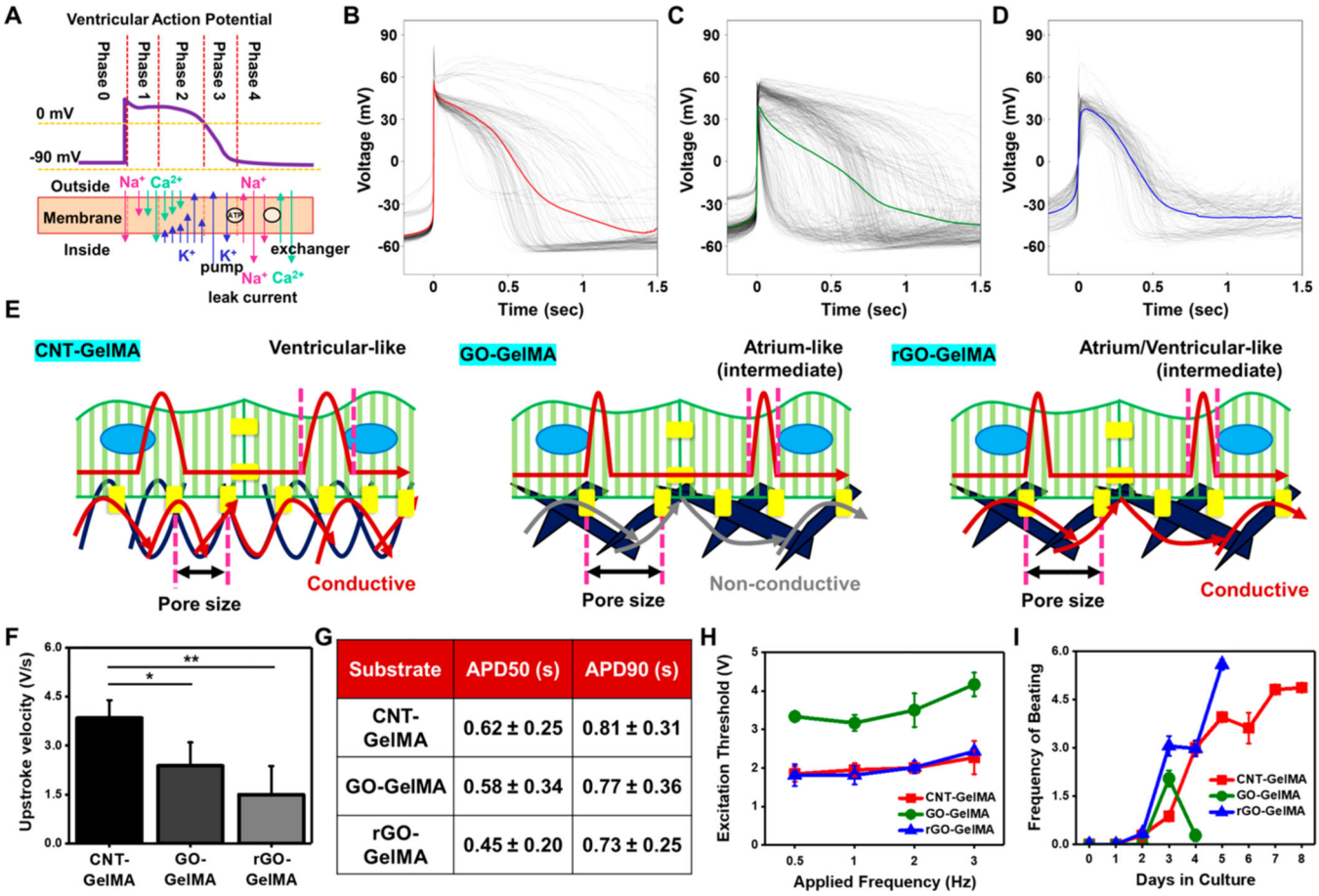

Substrate	APD50 (s)	APD90 (s)
CNT-GelMA	0.62 ± 0.25	0.81 ± 0.31
GO-GelMA	0.58 ± 0.34	0.77 ± 0.36
rGO-GelMA	0.45 ± 0.20	0.73 ± 0.25

Figure 5.

Phenotype of engineered cardiac tissues on hybrid scaffolds determined by electrophysiological properties. (A) Schematic representing the different phases of a ventricular action potential with inward and outward ionic currents. Action potential from cardiomyocytes cultured for 5 days on (B) CNT- (N = 4, # peaks = 140), (C) GO- (N = 8, # peaks = 494), and (D) rGO-GelMA (N =5, # peaks = 173). (E) Schematics displaying electric signal propagation through CNT, GO, and rGO links. CNT-GelMA with electric conductivity and better mechanical properties enables cardiomyocytes cultured on the surface to be like ventricular phenotypes. (F) Upstroke velocity and (G) action potential period evaluated at 50% (APD50) and 90% (APD90) for cardiomyocytes on CNT- (N = 4), GO- (N =8), and rGO-GelMA (N = 5). (H) Excitation threshold of engineered cardiac tissues on CNT-, GO-, and rGO-GelMA (N = 3). (I) Beating frequency of cardiac tissues evaluated from day 0 to 8 (N = 3). Error bars represent standard deviation.

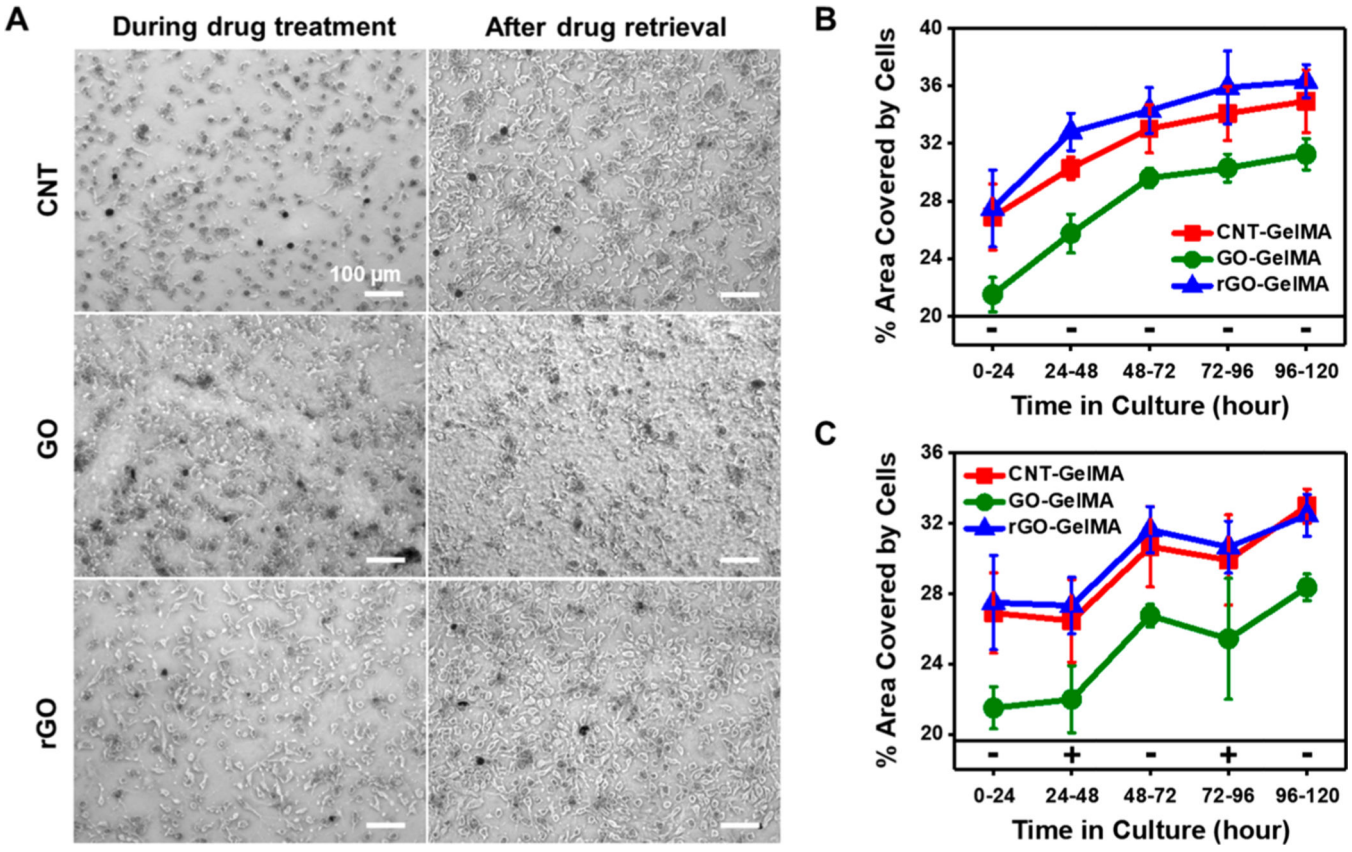

Figure 6.

Effect of contractility inhibition on cardiac tissue contraction on different hybrid scaffolds. (A) Optical images showing cardiomyocytes on CNT-, GO-, and rGO-GelMA during blebbistatin treatment and after drug retrieval. Percent area covered by cardiomyocytes (B) without drug treatment and (C) in the presence and absence of blebbistatin alternatively for 5 days ($N = 5$). Error bars represent standard deviation.

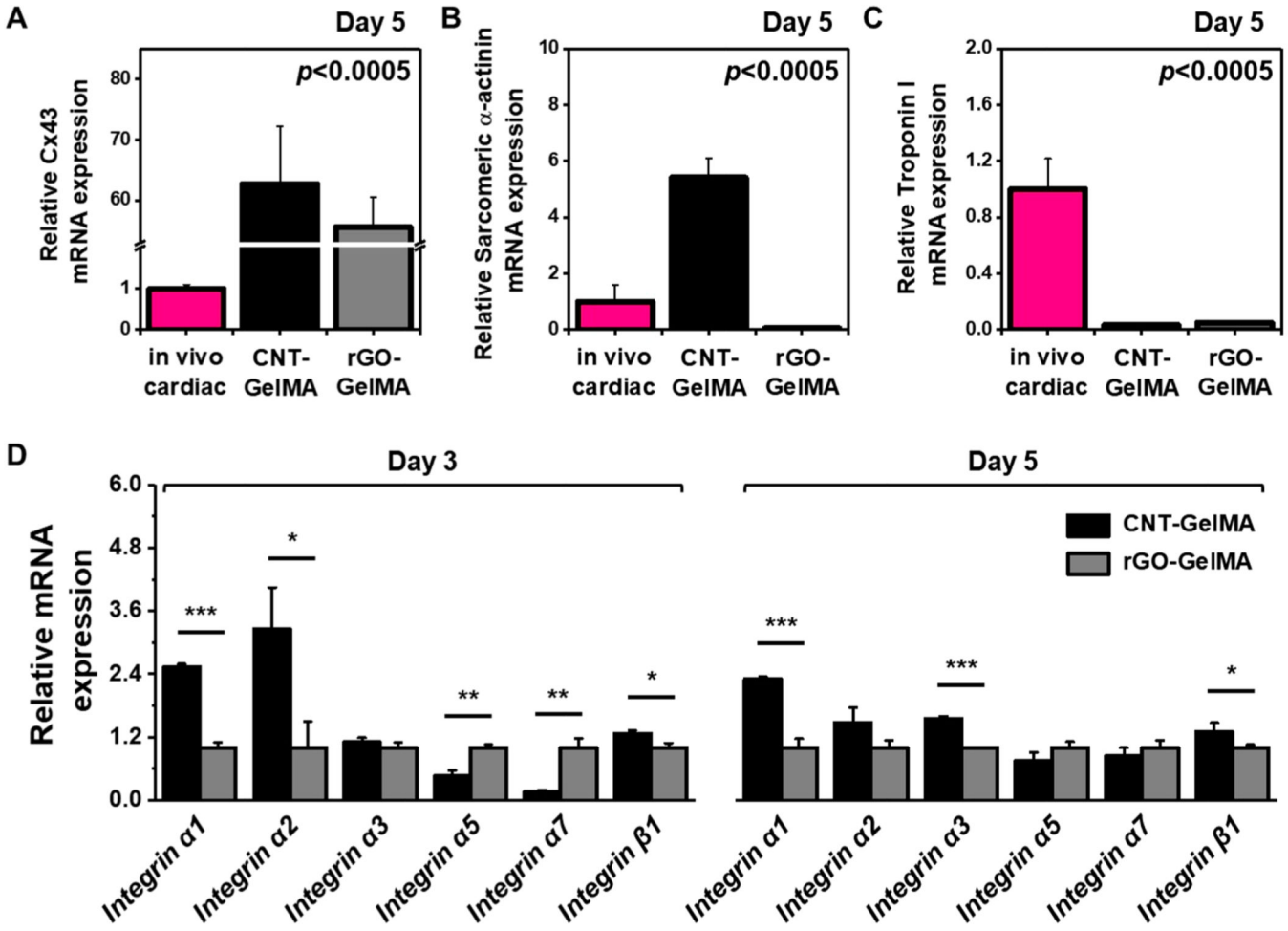

Figure 7.

Gene expression analysis of cardiac-specific transcripts and integrins. Results of qRT-PCR to measure the gene expression of cardiac-specific transcripts, (A) Cx43, (B) sarcomeric α-actinin, and (C) troponin I for cardiac tissues cultured on CNT- and rGO-GelMA compared with *in vivo* cardiac tissues ($N = 3$). (D) Results of qRT-PCR to measure the gene expression of integrins for cardiomyocytes cultured for 3 and 5 days on CNT- and rGO-GelMA ($N = 3$) (*$P < 0.05$, **$P < 0.005$, ***$P < 0.005$). Error bars represent standard deviation.

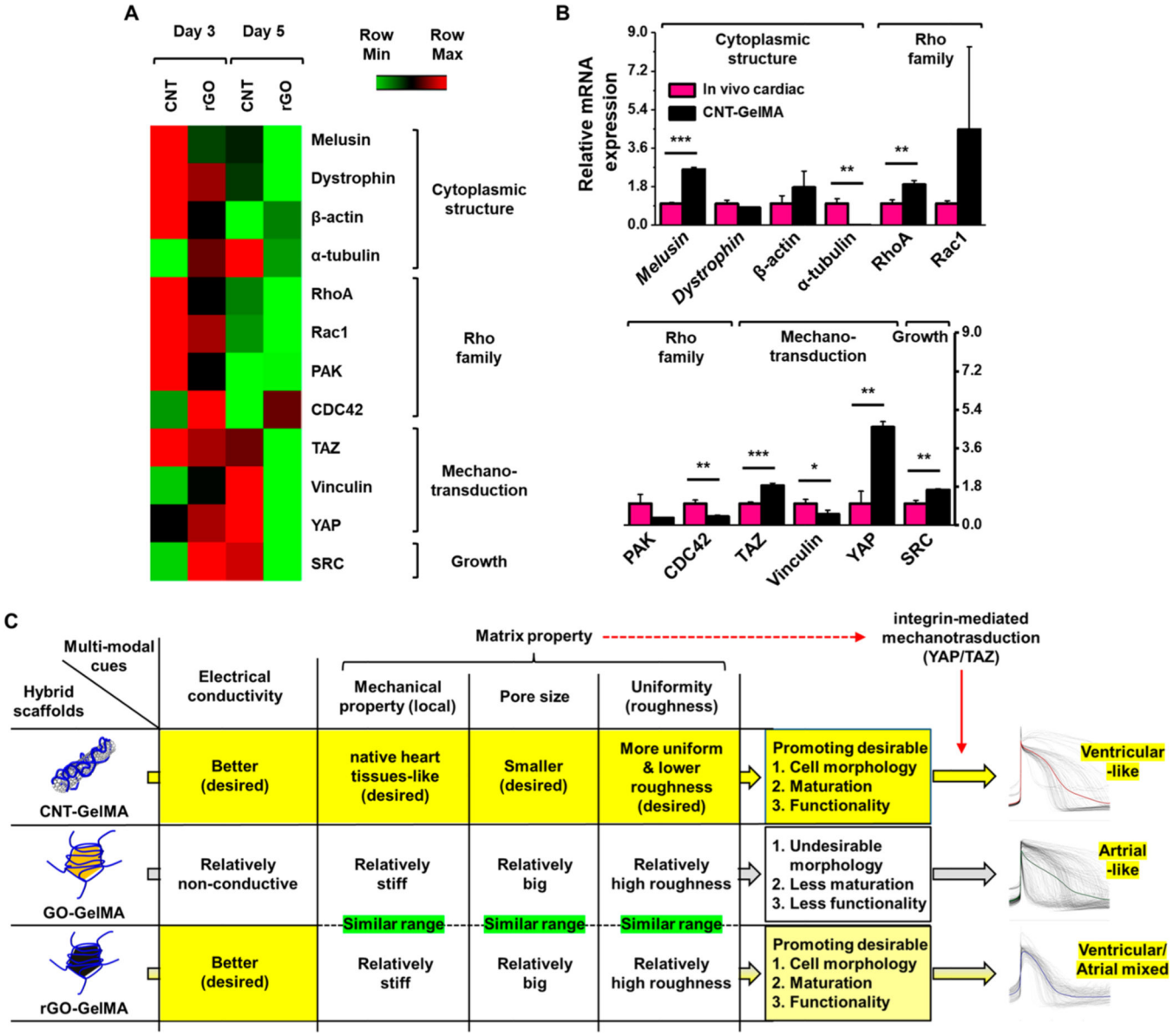

Figure 8.

CNT-GelMA guiding maturation of cardiac tissues through mechanotransduction signaling. (A) Heat map comparing a panel of transcripts linked to cytoplasmic structure, Rho family, mechanotransduction, and growth across cardiac tissues cultured for 3 and 5 days on CNT- and rGO-GelMA (N=3). (B) Results of qRT-PCR to measure the expression of genes employed in (A) for cardiac tissues matured for 5 days on CNT-GelMA compared to *in vivo* cardiac tissues (N= 3).(C) Summary of the effects of multimodal cues on cardiomyocyte maturation and functionality (*P < 0.05, **P < 0.005, ***P < 0.005). Error bars represent standard deviation.